Guanylate kinase 1 is an enzyme responsible for inosine accumulation in RNA of mammalian cells deficient in inosine triphosphatase

Tsuchimoto, Daisuke
Division of Neurofunctional Genomics, Advanced Research Initiative, Research Promotion Unit, Medical Institute of Bioregulation, Kyushu University

Takiguchi, Yuka
Division of Neurofunctional Genomics, Department of Immunobiology and Neuroscience, Medical Institute of Bioregulation, Kyushu University

Nakabeppu, Yusaku
Division of Neurofunctional Genomics, Department of Immunobiology and Neuroscience, Medical Institute of Bioregulation, Kyushu University

出版情報：Proceedings of the National Academy of Sciences. 123 (31), 2026-07-30. National Academy of Sciences
バージョン：

Guanylate kinase 1 is an enzyme responsible for inosine accumulation in RNA of mammalian cells deficient in inosine triphosphatase

Daisuke Tsuchimoto[a,b,1], Yuka Takiguchi[b], and Yusaku Nakabeppu[b]

[a]Division of Neurofunctional Genomics, Advanced Research Initiative, Research Promotion Unit, Medical Institute of Bioregulation, Kyushu University, Fukuoka, 8128582, Japan

[b]Division of Neurofunctional Genomics, Department of Immunobiology and Neuroscience, Medical Institute of Bioregulation, Kyushu University, Fukuoka, 8128582, Japan

[1]To whom correspondence may be addressed. Email: daisuke_nfg@kyudai.jp

Abstract

Inosine triphosphate (ITP) is a noncanonical nucleotide. Human cells possess inosine triphosphate pyrophosphatase (ITPA), and ITPA deficiency causes ITP accumulation within cells, leading to the onset of "Developmental and Epileptic Encephalopathy 35". Two potential pathways for ITP biosynthesis have been proposed: (i) oxidative deamination of the adenine base in adenosine triphosphate (ATP) or (ii) a two-step phosphorylation reaction of inosine monophosphate (IMP), an intermediate in the *de novo* synthesis of purine nucleotides. However, the mechanisms responsible for ITP biosynthesis in mammals remain unclear. In this study, using an *Itpa* knockout (KO) mouse cell line, we identified guanylate kinase 1 (*Guk1*) as a responsible gene for inosine accumulation in RNA. In *Itpa*-KO/*Guk1* knockdown (KD) cell lines, *Guk1* mRNA expression levels were positively correlated with the amount of inosine in RNA, most of which is incorporated during RNA synthesis in ITPA-deficient cells. The transient expression of human *GUK1* in *Itpa*-KO/*Guk1*-KD mouse cells significantly increased inosine levels in RNA. Recombinant human GUK1 phosphorylates IMP into inosine diphosphate (IDP). Furthermore, in brain-specific *Itpa*-KO mice, *Guk1* haploinsufficiency resulted in a significant reduction in inosine in cortical RNA and an extended lifespan. Thus, our results suggest that GUK1 is probably an enzyme responsible for ITP biosynthesis although the *K*m of GUK1 for IMP is very high *in vitro*.

Significance Statement

Living organisms possess enzymes that hydrolyze inosine triphosphate (ITP). In humans, inosine triphosphatase (ITPA) performs this function, and its deficiency leads to ITP accumulation and Developmental and Epileptic Encephalopathy 35 (DEE35). However, the ITP biosynthetic pathway has remained unresolved. We herein attempt to elucidate this pathway using cultured cells and genetically modified mice, providing insights into the mammalian nucleotide metabolism and the molecular basis of DEE35. This study sheds light on an unknown metabolic route linking it to disease *in vivo*.

Introduction

Inosine triphosphate (ITP) is hydrolyzed by specific enzymes (mammalian ITPA, *Escherichia coli* RdgB, budding yeast HAM1, etc.) within normal cells, converting it into inosine monophosphate (IMP) and pyrophosphate (1, 2). Consequently, it is an abnormal nucleotide present only at extremely low concentrations within the cells (3-6). However, ITP accumulates in mammalian cells lacking ITPA, suggesting that ITP is constantly generated in mammalian cells (7-9). Complete or severe ITPA deficiency causes humans to develop "Developmental and Epileptic Encephalopathy 35 (DEE35)" (6, 10, 11). DEE35 is characterized by microcephaly, developmental delay, growth retardation, and epileptic seizures. Some patients also exhibit dilated cardiomyopathy. There is no fundamental treatment for DEE35, and most patients die around 4 years of age or earlier. The disease is thought to result from the accumulation of ITP or deoxyinosine triphosphate (dITP). ITP competitively inhibits the ATP-binding site of myosin in the heart, leading to dilated cardiomyopathy (8, 12). Our studies using neural stem cell-specific *Itpa*-KO mice revealed that neuronal membrane potentials undergo depolarization in the brain, increasing the firing frequency of action potentials, which is thought to cause epileptic seizures (13). ITP accumulation in DEE35, due to its structural similarity to ATP and GTP (*SI Appendix*, Fig. S1), may antagonistically inhibit the actions of these normal purine nucleotides. Alternatively, as demonstrated for phosphatidylinositol 5-phosphate 4-kinase β and adenylsuccinate synthetase (14, 15), it may be utilized in their place. In addition to the direct effects of ITP, studies have shown that ITP is incorporated as a substrate during RNA synthesis, increasing inosine levels in RNA and impairing RNA functions, such as translation. RNA dysfunction is also hypothesized to cause disease (16). Cells lacking ITPA show instability in genomic DNA, likely due to the incorporation of dITP into DNA. We previously reported the accumulation of deoxyinosine in the DNA of ITPA-deficient primary mouse embryonic fibroblasts (7), although its level was nearly two orders of magnitude lower than that of inosine in RNA. Furthermore, Averill JR et al. demonstrated that human DNA polymerase eta can incorporate dITP into DNA *in vitro* (17). Another known substrate of ITPA is (deoxy)xanthosine triphosphate [(d)XTP]. However, to date, no reports exist on the accumulation of xanthosine/deoxyxanthosine in DNA/RNA or free XTP/dXTP in (d)ITP/(d)XTP hydrolase-deficient cells (6, 18). The ITP biosynthesis pathway has been proposed to involve either (i) oxidative deamination of ATP or (ii) two-step phosphorylation of IMP (*SI Appendix*, Fig. S2). In the latter pathway, the first step is the phosphorylation of IMP to inosine diphosphate (IDP). To date, *in vitro* IMP phosphorylation activities were reported in human erythrocyte-derived guanylate kinase and recombinant human adenylate kinase 6 (19, 20). However, there was no report to show what is the responsible enzyme for the phosphorylation of IMP *in vivo*. The second step is the phosphorylation of IDP, which was thought to be catalyzed by nucleoside diphosphate kinases (NME genes family products in human) (21). Some of them are considered "Non-specific" with respect to the base moiety

of substrate nucleotides (22-24). In this study, we identified guanylate kinase 1 (*Guk1*) as a gene essential for inosine accumulation in the RNA of ITPA-deficient mouse cells. We analyzed the role of GUK1 in ITP biosynthesis using purified recombinant human GUK1, ITPA-deficient cell lines, and ITPA-deficient mice. These results indicate that GUK1 is probably an enzyme responsible for ITP biosynthesis under physiological conditions.

Results

Establishment of a Neuro2a *Itpa*-KO clone and shRNA library screening

To elucidate the ITP production pathway in mammalian cells, we generated ITPA-deficient cells in which ITP accumulated intracellularly. Using mouse neuroblastoma-derived Neuro2a cells as the original ITPA-proficient cells, we obtained four candidate Neuro2a *Itpa*-KO cell clones using CRISPR/Cas9 and a TIDE analysis, as described in the Materials and Methods section. The ITPA protein expression in these clones was confirmed by western blotting using an anti-ITPA antiserum. Ultimately, Clone #1-16-9 was selected as the Neuro2a *Itpa*-KO cell line for subsequent experiments (Fig. 1A, *SI Appendix*, Fig. S3). Next, we hypothesized that the ITP biosynthesis pathway in mammalian cells under physiological conditions involves a two-step phosphorylation of intracellular IMP. To analyze this pathway, we decided to promote it by increasing the concentration of IMP. Pang et al. demonstrated that the suppression of IMP consumption via genetic mutations in *E. coli* and yeast leads to increased ITP production. Furthermore, a study by Vidal et al. showed that adding hypoxanthine increases IMP production via salvage synthesis, while simultaneously inhibiting IMP dehydrogenase 1 and 2 to inhibit IMP consumption, thereby specifically suppressing the proliferation of *Trypanosoma* ITPA-deficient strains (18, 25). Based on these results, we implemented HMGA treatment by adding four types of additives to the culture medium (Fig. 1B). For HMGA treatment, hypoxanthine, mycophenolic acid, guanosine, and adenosine were added to Neuro2a *Itpa*-KO cell culture medium. Hypoxanthine is converted to IMP by hypoxanthine phosphoribosyltransferase 1 (HPRT1), an enzyme involved in the salvage pathway. The addition of mycophenolic acid inhibits IMP dehydrogenase 1 and 2, thereby suppressing the conversion of IMP to GMP (i.e., the consumption of IMP). Guanosine is converted to GMP via guanine through the HPRT1-dependent salvage pathway, compensating for the reduced GMP production caused by mycophenolic acid, thereby preventing cell death induced by mycophenolic acid treatment. Adenosine is converted to AMP via adenine through an adenine phosphoribosyl transferase (Aprt)-dependent salvage synthesis pathway. AMP inhibits adenylosuccinate synthetase 1 and 2 (ADSS1, ADSS2), which catalyzes the first step of conversion from IMP to AMP via negative feedback inhibition, thereby further suppressing IMP consumption (26, 27). We anticipated that HMGA treatment would cause IMP accumulation and promote ITP

biosynthesis via a 2-step phosphorylation. Hypoxanthine, guanosine, and adenosine, individually added at 1000, 250, and 250 μM, respectively, did not specifically inhibit the proliferation of Neuro2a *Itpa*-KO cells over four days relative to control Neuro2a cells (Fig. 1C). HMGA treatment with all these components and mycophenolic acid suppressed Neuro2a cell proliferation by approximately half. In contrast, proliferation in Neuro2a *Itpa*-KO cells was strongly suppressed to approximately 5.8%, demonstrating a statistically significant Neuro2a *Itpa*-KO-specific inhibitory effect ($p < 0.0001$). To check the effects of HMGA treatment, we cultured Neuro2a *Itpa* KO cells for 2 days with or without HMGA and analyzed their extract by high performance liquid chromatography (HPLC). As a result, we detected an HMGA-specific peak near the retention time of IMP standard. The UV spectra of the peak was similar to but different from that of IMP (*SI Appendix* Fig. S4A and B). Thus, we could not confirm the increase in IMP levels by HMGA treatment. Regarding ITP, we could not detect any ITP peak in the HPLC chromatograph (*SI Appendix* Fig. S4C). Kevelam et al. reported that they detected ITP in the red blood cells of patients with ITPA deficiency, but were unable to detect ITP in fibroblasts derived from these patients (10). We also previously detected ITP in the erythrocytes of ITPA deficient mice by HPLC, but not in their other tissues (8). Our result in the present study is consistent with the previous reports. Therefore, we measured the inosine levels in RNA from Neuro2a *Itpa* KO cells by an HPLC analysis of RNA digests, using them as an indicator of the intracellular ITP levels. The results showed that the inosine levels in RNA increased fourfold in HMGA-treated *Itpa* KO cells compared with untreated cells (*SI Appendix* Fig. S5). Based on this finding, we hypothesized that HMGA treatment enhances ITP biosynthesis. To identify genes involved in ITPA-deficiency-specific cell growth inhibition, positive screening was performed using mouse shRNA lentiviral libraries (Cellecta) (Fig. 1D). The libraries consisted of Mouse module 1 (signaling pathway) and Mouse module 2 (disease-associated). First, Neuro2a *Itpa*-KO cells were separately infected with mouse shRNA lentiviral libraries for Modules #1 and #2. Cells immediately post-infection were designated as mModule#1-cont and mModule#2-cont. After four weeks of culture in the presence of HMGA, most cells either ceased proliferating or died. However, a subset of the cells continued to proliferate and formed multiple colonies. Following HMGA treatment, these cells were recovered and designated as mModule1-HMGA and mModule2-HMGA. Genomic DNA was extracted from each of the cell samples. The shRNA-coding region of the lentiviral vector integrated into the genomic DNA was amplified by PCR and analyzed by MiSeq NGS, yielding shRNA-coding sequence count information for each genomic DNA sample (28,403 counts from mModule1-cont, 32,202 counts from mModule1-HMGA, 27,762 counts from mModule2-cont, and 29,777 counts from mModule2-HMGA, Dataset S1) (Step 1). Next, for the analysis of the obtained count data, we selected shRNA coding sequences that were counted at least 10 times in the HMGA-treated samples and further showed a tenfold or greater increase in frequency when comparing before and after HMGA treatment (Dataset S2 and S3) (Step 2). Finally, NCBI BLAST analysis of mouse mRNAs containing target sequences for the

shRNAs selected in step 2 revealed that only three genes were targeted by multiple selected shRNAs (Table 1). Among these, mouse *Guk1* (*mGuk1*) was targeted by four different types of shRNA sequences (*SI Appendix*, Table S1), whereas the others were targeted by two. Guanylate kinase 1 (GUK1) encoded by the *mGuk1* gene is known to phosphorylate GMP using ATP as a phosphate donor, producing GDP (28). As described above, human erythrocyte-derived guanylate kinase and human recombinant adenylate kinase 6 are known to phosphorylate IMP *in vitro*. Therefore, GUK1 might be responsible for the phosphorylation step from IMP to IDP in the two-step phosphorylation hypothesis for intracellular ITP biosynthesis (*SI Appendix*, Fig. S2B).

Establishment and analysis of Neuro2a *Itpa*-KO/*Guk1*-KD cells

To confirm the role of GUK1 in ITP biosynthesis *in vivo*, Guk1-KD clones (Neuro2a *Itpa*-KO/*Guk1*-KD) stably expressing *Guk1* shRNA were established using Neuro2a *Itpa*-KO#1-16-9 cells. The *Guk1* shRNA target sequence employed was that of the shRNA that exhibited the highest detection frequency after HMGA treatment during shRNA library screening (Target mGuk1variant 5 exon3/4: GATGGCAAAGATTACTACTTT in *SI Appendix*, Table S1 and S2). After transfection of the shRNA plasmid, 11 stable clones were established, as described in the Materials and Methods section. The *Guk1* mRNA expression levels in 11 clones were analyzed and compared using real-time PCR. The results showed that clones #11 and #13 expressed 31.8% and 8.2% of *Guk1* mRNA, respectively, relative to control Neuro2a *Itpa*-KO cells (*SI Appendix*, Table S3). Lower GUK1 protein levels were also confirmed by western blotting of these clones (Fig. 2A and *SI Appendix.* Fig. S3). Furthermore, cell proliferation during the 4 days of HMGA treatment was examined in clones #11 and #13. Relative to ITPA proficient Neuro2a cells, Neuro2a *Itpa*-KO cells exhibited more severe proliferation inhibition upon HMGA treatment ($p < 0.0001$) (Fig. 2B and *SI Appendix*, Fig. S6). In contrast, Neuro2a *Itpa*-KO/*Guk1*-KD #11 and #13 exhibited significantly alleviated growth inhibition during HMGA treatment ($p < 0.0001$ vs. Neuro2a *Itpa*-KO cells). Next, we analyzed the inosine content of RNA as an indicator of intracellular ITP levels. The results showed that, in Neuro2a cells, RNA inosine was below the detection limit (< 21 Ino/10^6 Guo), whereas Neuro2a *Itpa*-KO cells exhibited a marked increase in Ino content at 1100 Ino/10^6 Guo (Fig. 2C and *SI Appendix*, Fig. S7). This level was comparable to that previously reported by us in ITPA-deficient tissues from *Itpa* conditional KO (cKO) mice (2230 Inosine/10^6 Guo in cortex) (13). Following two days of HMGA treatment in these cells, a slight detection of inosine was observed even in Neuro2a cells. In Neuro2a *Itpa*-KO cells, HMGA treatment significantly increased the Ino content in RNA by approximately four-fold (4698 Ino/10^6 Guo) again as well as the data in *SI Appendix*, Fig. S5. In contrast, Ino levels in RNA from Neuro2a *Itpa*-KO/*Guk1*-KD clones #11 and #13 were significantly decreased after HMGA treatment (3291 Ino/10^6 Guo and 1331 Ino/10^6 Guo, both $p < 0.0001$, vs. *Itpa*-KO [HMGA]). More strikingly, under standard culture conditions without HMGA treatment, Ino levels in Neuro2a *Itpa*-KO/*Guk1*-KD #11

and #13 cells decreased to 24.4% and 10.0%, respectively, relative to Neuro2a *Itpa*-KO cells (268 Ino/10^6 Guo and 110 Ino/10^6 Guo, both $p < 0.0001$). Next, inosine levels in RNA were measured for all Neuro2a *Itpa*-KO/*Guk1*-KD 11 clones and the parental Neuro2a *Itpa*-KO #1-16-9 cells and plotted alongside *Guk1* mRNA expression levels. (Fig. 2D) The results showed a strong positive correlation between Ino levels in RNA and *Guk1* mRNA expression levels (Pearson's correlation coefficient between them was 0.979529). Ino RNA is present at very low levels in WT cells and mouse tissues, whereas it is markedly increased in ITPA-deficient cells and ITPA-deficient mouse tissues. Accumulated ITP is thought to be incorporated as a substrate during RNA synthesis (7, 13). Thus, our results demonstrated that GUK1 probably plays an essential role in intracellular ITP biosynthesis under physiological conditions. Next, when a human GUK1 expression plasmid was transiently introduced into clone #13, which exhibited the lowest mouse *Guk1* mRNA expression level, as described above, the Ino content of RNA was markedly increased relative to the vector-control three days after transfection (Fig. 2E). This indicates that the positive correlation between Ino levels and *Guk1* mRNA levels is not due to off-target effects of *Guk1* shRNA, but is indeed due to the changed *Guk1* mRNA /GUK1 protein levels. Furthermore, this correlation is common to both mouse GUK1 and human GUK1 proteins.

Analysis of recombinant human GUK1 protein

In 1971, Agarwal et al. reported that guanylate kinase extracted and purified from human erythrocytes exhibited the ability to phosphorylate IMP to IDP in addition to its intrinsic substrate GMP. Although the activity in this report was highly likely attributable to the product of the human *GUK1* gene (*hGUK1*), confirmation was not possible at the time, as the *hGUK1* gene had not yet been cloned. Therefore, to demonstrate the IMP phosphorylation activity of GUK1, we isolated *hGUK1* variant 2 cDNA and prepared recombinant N-terminally His-tagged hGUK1 isoform b protein (His-hGUK1) using the methods described in the Materials and Methods section. Purified His-hGUK1 was recognized as a single band by silver staining on an SDS-PAGE gel (Fig. 3A and *SI Appendix*, Fig. S8). Using the purified His-hGUK1, phosphorylation reactions with GMP and IMP were performed. Similar to Agarwal et al., the phosphorylation reaction product using ATP as the phosphate donor was coupled with reactions involving pyruvate kinase and lactate dehydrogenase (*SI Appendix*, Fig. S9). Reaction rates were monitored as decreases in NADH absorbance, and K_m and k_{cat} values were determined using Hanes-Woolf plots (GMP and IMP) (*SI Appendix*, Fig. S10 and Fig. 3B). Next, reactions were performed without pyruvate kinase and lactate dehydrogenase to identify the reaction products, GDP, and IDP. The products were analyzed by HPLC and the absorbance peaks were compared with the standard sample peaks in the retention time and UV spectrum. Recombinant His-hGUK1 produced IDP upon IMP phosphorylation (Fig. 3C, 3D), and exhibited K_m values of 93.3 μM GMP and 2005 μM IMP (Table 2). These results are largely consistent with the measurements of

endogenous guanylate kinase by Agarwal et al. (GMP K_m: 77 μM, IMP K_m: 1300 μM). The slightly higher K_m values may be due to the influence of N-terminal HisTag. Regarding k_{cat}, GMP k_{cat} (s^{-1}) was 17.6 and IMP k_{cat} (s^{-1}) was 0.588. Thus, IMP exhibited approximately 3% of the GMP value, which was slightly higher than the 0–2% range reported by Agarwal et al.

Analysis of *Itpa*$^{flox/flox}$/*Nes-Cre*/*Guk1*$^{+/-}$ mice

We employed *Guk1* KO mice (C57BL/6NJ-Guk1<em1(IMPC)J, established in MMRRC at The Jackson Laboratory) to investigate the contribution of GUK1 to ITP biosynthesis in mammalian animals. The International Mouse Phenotype Consortium (IMPC) (https://www.mousephenotype.org/) reports that homozygous *Guk1*$^{-/-}$ mice exhibit 'preweaning lethality with complete penetration.' To confirm lethality, we crossed *Guk1*$^{+/-}$ female and male mice and examined the genotype of newborn offspring mice. As shown in *SI Appendix*, Table S4, no *Guk1*$^{-/-}$ mice were identified, suggesting embryonic lethality in homozygotes with complete penetration. We then crossed the previously established *Itpa*$^{+/flox}$/*Nes-Cre* mice with *Guk1*$^{+/-}$ mice to obtain *Itpa*$^{+/flox}$/*Nes-Cre*/*Guk1*$^{+/-}$ mice. Crossing these lines with *Itpa* (flox/flox) mice yielded eight distinct genotypes. The birth ratios of the eight genotypes showed no significant differences (*SI Appendix*, Table S5). Among the mice obtained, female *Itpa*$^{flox/flox}$ mice, *Itpa*$^{flox/flox}$/*Nes-Cre* mice, and *Itpa*$^{flox/flox}$/*Nes-Cre*/*Guk1*$^{+/-}$ mice, were used to compare the expression levels of GUK1 and ITPA proteins in the cerebral cortex at P17 or P18 by western blotting. ITPA was almost absent in the cortex of *Itpa*$^{flox/flox}$/*Nes-Cre* mice. The residual ITPA signal is thought to originate from microglia and vascular cells, which are not derived from neural stem cells. In *Itpa*$^{flox/flox}$/*Nes-Cre*/*Guk1*$^{+/-}$ mice, GUK1 protein levels were reduced by approximately half (Fig. 4A). As previously reported, neural stem cell-specific ITPA-deficient mice (*Itpa* cKO: *Itpa*$^{flox/flox}$/*Nes-Cre* mice) show growth retardation and weight loss one week after birth and die approximately three weeks after birth (13). *Itpa*$^{flox/flox}$/*Nes-Cre* /*Guk1*$^{+/-}$ mice showed no statistically significant difference in body weight at P17 relative to *Itpa* cKO mice (*Itpa*$^{flox/flox}$/*Nes-Cre* mice), by a 2-way ANOVA after aligned rank transform ($p = 0.4546$) or the *Guk1* genotype effect test ($p = 0.2884$) (Fig. 4B). In contrast, when comparing survival rates, the median survival period for *Itpa*$^{flox/flox}$/*Nes-Cre* mice changed from 21 days to 25 days after *Guk1* haploinsufficiency, showing a statistically significant increase in lifespan (Log-Rank test, $p < 0.0001$) (Fig. 4C). Next, we analyzed Ino levels in the RNA. Ino levels in the cerebral cortex of *Itpa*$^{flox/flox}$/*Nes-Cre*/*Guk1*$^{+/-}$ mice were significantly lower than those in *Itpa*$^{flox/flox}$/*Nes-Cre* mice ($p = 0.0008$, Wilcoxon signed-rank test) (Fig. 4D). This suggests that the reduced expression of GUK1 probably led to decreased ITP biosynthesis, thereby mitigating the short lifespan of ITPA-deficient mice. In 2024, four patients with mitochondrial DNA depletion syndrome were reported in humans, caused by mutations in both alleles of the human *GUK1* gene, resulting in a reduction in GUK1 activity in fibroblasts to less than half of that in healthy controls (29). Because this paper mentions the low birth

weight of the patients, we also examined the effect of the *Guk1* KO allele on the body weight of the mice at P14. A two-way ANOVA after aligned rank transform (p = 0.1863) revealed that the *Guk1* genotype effect was significant (p = 0.0362), while the sex effect was not significant (p = 0.7939). There was no interaction between these effects (p = 0.6857). This result showed a lower body weight in $Guk1^{+/-}$ mice than in $Guk1^{+/+}$ mice (Fig. 4E). This suggests that in addition to the lymphopenia reported by The Jackson Laboratory, *Guk1* haploinsufficiency might cause various systemic phenotypes, including reduced body weight, which were observed in patients with GUK1-deficiency and are thought to be due to a decreased dGTP concentration in the nuclei and mitochondria (29). Furthermore, these results suggest that the reason why the low body weight in *Itpa* cKO mice at P17 was not significantly restored by *Guk1* haploinsufficiency might be that the restorative effect was masked by the weight loss caused by *Guk1* haploinsufficiency itself.

Discussion

We previously analyzed the effects of ITP accumulation in mammals using cultured cells and an ITPA-deficient mouse model. As a result, we elucidated molecular pathologies such as genomic instability, dilated cardiomyopathy due to sarcomere structural disruption and convulsive seizures due to depolarization of the resting membrane potential in neurons (7, 8, 13). However, we considered that elucidating the pathway for ITP production, the causative agent, is necessary for treating DEE35 patients. Two potential pathways for ITP generation *in vivo* have been proposed: (i) oxidative deamination at the 6th carbon position of the adenine base in ATP or (ii) a two-step phosphorylation reaction of IMP, an intermediate in the purine nucleotide *de novo* synthesis pathway (*SI Appendix*, Fig. S2). In the former pathway, low pH and nitric oxide (NO) or nitrite are thought to promote the reaction, and an increase in dIno within DNA due to the reaction between DNA and NO has been reported (30). Furthermore, Prestwich et al. reported increased inosine in RNA due to NO production from macrophages and neutrophils in an SJL mouse model of excessive NO production following transplantation of RcsX lymphoma cells (31). This suggests that oxidative deamination reactions occur on the adenine base within DNA or RNA, or within ATP as an RNA substrate *in vivo*, resulting in the formation of (deoxy)inosine. Meanwhile, in non-mammalian microorganisms such as *E. coli* and *Saccharomyces cerevisiae*, it has been reported that defects in the IMP consumption pathways to GMP or AMP lead to increased levels of dIno in DNA and rIno in RNA (18). It is thought that IMP accumulated due to the consumption pathway defect undergoes two-step phosphorylation to form ITP or dITP, which is then incorporated during RNA or DNA synthesis. In plants, the administration of inhibitors targeting IMP metabolic enzymes IMP dehydrogenase 1 and 2 in ITP hydrolyzing enzyme-deficient strains, or growth in the presence of cadmium sulfate, has been reported to increase ITP. This

confirms the existence of both ITP production pathways in plants (32). Thus, two distinct ITP production pathways (ATP oxidative deamination and IMP phosphorylation) have been suggested. However, the pathway that plays the primary role in ITP production under physiological conditions in mammalian cells remains unclear. We hypothesized that the two-step phosphorylation of IMP is likely the primary ITP production pathway in mammalian cells, as the conditions promoting oxidative deamination from ATP (i.e., low pH and high concentrations of nitrite or NO) do not appear to be physiological for most mammalian tissues and cells. The phosphorylation of IMP has been reported with purified human erythrocyte-derived guanylate kinase and recombinant ADK6 (19, 20), although their roles in ITP-biosynthesis *in vivo* had not been elucidated. To expect IMP accumulation, we devised an HMGA treatment and identified *Guk1* as an essential gene for inosine accumulation in the RNA of *Itpa*-KO cells through screening using a mouse shRNA lentiviral library. As anticipated, HMGA treatment increased inosine levels in the RNA of ITPA-deficient cells. Furthermore, *Guk1*-KD reduced not only the HMGA-induced increase in RNA inosine, but also the accumulation of RNA inosine under normal culture conditions. This suggests that ITP biosynthesis in mammalian cells under physiological conditions probably depends on GUK1. In this pathway, IMP may be converted to IDP, and then to ITP by GUK1 and nucleoside diphosphate kinases, respectively.

As described above, two mammalian enzymes have been proposed as candidates for converting IMP to IDP: erythrocyte-derived guanylate kinase and adenylate kinase 6. Using genetic approaches, this study suggests that GUK1 is probably responsible for ITP biosynthesis. Using recombinant His-tagged hGUK1 prepared in-house, we found the K_m value for IMP to be 2005 μM, which is similar to the K_m value of 1300 μM reported for erythrocyte-derived guanylate kinase (19). These K_m values appear excessively high considering that IMP levels in human cells are reported to be approximately 1% of ATP levels (33, 34), raising doubts about whether the reaction actually proceeds *in vivo*. Agarwal et al. have suggested the possibility of increased activity through allosteric regulation (19). Recently, Schneider et al. reported that phosphorylation of tyrosine residue 74 in the GUK1 protein increases GMP phosphorylation activity (35). It would be intriguing to consider how tyrosine phosphorylation might affect GUK1 IMP phosphorylation activity. Furthermore, Wolfe et al. have reported that enzymes from the purine *de novo* synthesis pathway complex (purinosome) and the GTP synthesis pathway, including GUK1, co-localize at the cell leading edge within human renal carcinoma cell lines (36). The former includes phosphoribosyl pyrophosphate synthetase (PRPS), phosphoribosyl pyrophosphate amidotransferase (PPAT), phosphoribosylglycinamide formyltransferase (GART), phosphoribosyl formylglycinamidine synthase (FGAMS), phosphoribosyl aminoimidazole succinocarboxamide synthetase (PAICS), adenylosuccinate lyase (ADSL), and 5-amino-4imidazolecarboxamide ribonucleotide transformylase/IMP cyclohydrolase (ATIC), all of which are involved in IMP *de novo* synthesis. Consequently, IMP concentrations higher than the intracellular average may coexist with GUK1 at localized sites such as the cell leading edge.

Furthermore, it has been reported that intracellular IMP concentrations increase markedly in human skeletal muscle and erythrocytes during rapid ATP consumption (33, 37). Thus, it is conceivable that IMP reaches high concentrations in specific cells or intracellular localities under certain conditions, potentially serving as a GUK1 substrate. Regarding dITP, IDP produced by GUK1 may be further converted to dIDP and then to dITP, at least in *Saccharomyces cerevisiae* and *Escherichia coli*. This is supported by observations that defects in the IMP consumption pathways lead to the accumulation of deoxyinosine (dI) in DNA in these organisms (18). An alternative pathway for dITP biosynthesis may involve the two-step phosphorylation of deoxyinosine monophosphate (dIMP), a degradation product of DNA. In this pathway, GUK1 could catalyze the conversion of dIMP to dIDP, as human guanylate kinase has been shown to phosphorylate deoxyguanosine monophosphate (dGMP) to deoxyguanosine diphosphate (dGDP) (19).

This study showed that GUK1 plays a role in inosine accumulation in RNA in cultured cells and mice, particularly in the absence of ITPA. This supports the two-step phosphorylation hypothesis for the generation of ITP from IMP although there is no direct evidence of phosphorylation of IMP by GUK1 *in vivo*, and *K*m of GUK1 for IMP is very high *in vitro*. In ITPA-deficient mice, a model of DEE35, *Guk1* haploinsufficiency extended lifespan and reduced the median inosine level in RNA to 66.6% of that in the controls. This suggests that even a 50% reduction in the GUK1 activity probably lower the ITP levels in a biologically meaningful manner, thus leading to improved survival. However, both our results and those from The Jackson Laboratory indicate that Guk1 haploinsufficiency has harmful effects. This implies that the strong inhibition of GUK1 may be toxic to mammals. Therefore, although GUK1 is a potential therapeutic target for DEE35, targeting it safely may be difficult.

Materials and Methods

HMGA (hypoxanthine, mycophenolic acid, guanosine, and adenosine) treatment and viability assay of cultured cells

Cells seeded at a density of 2000 cells/well in a 96-well plate were treated with hypoxanthine, mycophenolic acid (Fujifilm), guanosine, and adenosine to achieve final concentrations of 1 mM, 10 μM, 250 μM, and 250 μM, respectively (HMGA treatment). After 96 h of culture, an equal volume of medium containing 10% Cell Counting Kit 8 (Dojindo, Kumamoto, Japan) was added. Viability was assessed by measuring the OD450-600 after 2 h of further culture.

Preparation of cell extracts for nucleotides analysis

Cell extracts were prepared for the analysis of intracellular nucleotides. The cells were harvested by treatment with trypsin and ethylenediaminetetraacetic acid (EDTA) (Sigma-Aldrich) and washed with D-PBS (-) (Fujifilm). Pellets of 5×10^6 cells for each sample were prepared by centrifugation and lysed by the addition of 100µl of 0.42M HClO4 supplemented with 1% phosphatase inhibitor cocktail (Nacalai Tesque, Kyoto, Japan) and 1% deoxycoformycin (Santa Cruz Biotechnology, Inc., Dallas, Texas, USA). After centrifugation at 20000 × *g* for 5min at 4°C, 100µl of supernatant was mixed with 33µl of 3M K2HPO4 and centrifuged again at 20000 × *g* for 5 min at 4°C. The supernatants were subjected to an HPLC analysis after 15-fold dilution to decrease the concentration of salts.

HPLC analysis of nucleotides

With a Prominence 20 HPLC system connected to a TSKgel ODS-100V 3 µm column 2 × 150 mm (Tosoh, Tokyo, Japan), separation of the nucleotides in the samples was performed in gradient mode (20 mM t-butylamine, pH 6.8 with H_3PO_4, 0%–10% methanol over 40 min or 0%-6.2% methanol over 50min), with detection by a DIODE ARRAY DETECTOR. Each nucleotide was confirmed by comparing the retention time and UV spectrum of the product peak with those of the standard nucleotide samples.

RNA extraction and digestion for the HPLC analysis

RNA was extracted from cultured cells and the mouse cerebral cortex using the RNeasy Mini Kit and RNeasy Lipid Tissue Mini Kit (Qiagen), respectively. During extraction, 20 mM 2,2,6,6-tetramethylpiperidine 1-oxyl (TEMPO) and 300 µM deoxycoformycin were added to the samples. Subsequently, 100 µM deoxycoformycin was added during the extraction process, and the final elution was performed with nuclease-free water (Nacalai Tesque). RNA was quantified by measuring the OD260, and 30 µg of each sample was digested following the modified protocol described by Taghizadeh et al. (9) (7). The digestion products were diluted with an equal volume of H_2O, filtered through an Ultrafiltration Spin Column 3 K (Pharma Foods), and analyzed using a Prominence 20 HPLC system (Shimadzu, Kyoto, Japan) connected to a YMC Hydrosphere C18 column 2 × 150 mm (YMC, Kyoto, Japan). The nucleosides were separated in the isocratic mode (100% H_2O, 40 min) and then were detected using a DIODE ARRAY DETECTOR (SPD-M20A, Shimadzu). Calibration curves were created from the peak areas of the chromatograms for the Guo and Ino reference standards, and Guo and Ino in the products were quantified.

ShRNA library preparation and infection screening

The preparation of pseudovirus particle solutions and titer checks were performed with Cellecta Decipher shRNA lentiviral library pRSI9-u6-(sh)-UbiC-TagRFP-2A-Puro Mouse Module 1 (signaling pathway) and Mouse Module 2 (disease-associated) DNA (Cellecta, Mountain View, CA, USA) and

HEK293T cells, according to Cellecta's protocol. Modules #1 and #2 were independently infected into 1.0×10^7 Neuro2a *Itpa*-KO cells suspended in 25 ml of medium containing 10 μg/ml hexadimethrine bromide (Sigma-Aldrich) to achieve a transduction efficiency of 35%. The cells were then seeded into two separate 150 mm Nunc culture dishes (Thermo Fisher Scientific). At 24 h post-infection, the medium was replaced with a standard medium. At 48 h post-infection, cells were harvested from one of the two dishes to serve as HMGA-untreated control samples (mModule1-cont and mModule2-cont). Simultaneously, the medium in the remaining dishes was replaced with HMGA-supplemented medium to initiate the screening. HMGA-supplemented medium was replaced every 2-3 days. After 4 weeks, HMGA-treated cells (mModule1-HMGA and mModule2-HMGA) were harvested, and genomic DNA was extracted. For next-generation sequencing (NGS), the 1st PCR (340 bp, including the adapter sequence) for the shRNA coding region was performed using MightyAmp DNA Polymerase (Takara-Bio) and the adapter-containing primer set Fw1 for shRNA with adaptor/GexSeqN with adaptor (*SI Appendix*, Table S2). Second-round PCR, using the first PCR product as a template, and NGS (2 × 300 bp) with the MiSeq system and MiSeq Reagent Kit v3 (Illumina, San Diego, CA, USA) were performed by Bioengineering Lab. Co. Ltd., (Kanagawa, Japan).

Establishment of Neuro2a *Itpa*-KO/*Guk1*-KD cells

Using Neuro2a *Itpa*-KO cells, Neuro2a *Itpa*-KO/*Guk1*-KD clones stably expressing mouse *Guk1* (*mGuk1*) shRNA were established as follows. First, an shRNA expression plasmid targeting the sequence of the *mGuk1* gene, target mGuk1variant 5 exon3/4 (the exon3/exon4 junction sequence of mouse *Guk1* mRNA variant 5 [NCBI Reference Sequence: NM_001403835.1]) (*SI Appendix*, Table S2), was constructed as follows. Oligomeric DNA Guk1 sh ins#1 and Guk1 sh ins#2 (*SI Appendix*, Table S2) were annealed and inserted into the cloning site of pRNAi-mU6-green (Biosettia, San Diego, CA) using Ligation Mix (Takara-Bio, Mighty Cloning Kit). The resulting pRNAi-mU6-green: *mGuk1*-shRNA was introduced into Neuro2a *Itpa*-KO cells along with a Linear Hygromycin Marker (Takara-Bio) using the above-described method. The cells were cultured and selected in the presence of Hygromycin B (300 μg/ml), and the resulting colonies were isolated (Neuro2a *Itpa*-KO/*Guk1*-KD). RNA extraction and cDNA synthesis for each clone were performed using ReverTraAce qPCR RT Master Mix with gDNA remover (Toyobo). Mouse *Guk1* mRNA and *Rps18* mRNA (internal control) expression levels were quantified and compared using cDNA samples, Thunderbird Next SYBR qPCR Mix (Toyobo), and the Thermal Cycler Dice Real Time System TP870 (Takara-Bio). The PCR primer sets used for these amplifications were mGuk1 Fw6/mGuk1 Rv6 and Mmu Rps18-F/Mmu Rps18-R, respectively (*SI Appendix*, Table S2).

Human *GUK1* cDNA cloning and construction of its expression vectors

To prepare the recombinant protein, human *GUK1* (*hGUK1*) mRNA variant 2 (NCBI Reference

Sequence: NM_000858.7) coding for human GUK1 isoform b protein, which has been reported as a cytoplasm-localizing isoform (29), was amplified from the total cDNA of HeLaMR cells (38) using the primer set NdeI-hGUK1 Fw/hGUK1 Rv-HindIII (*SI Appendix*, Table S2) and Tks Gflex DNA polymerase (Takara Bio). This cDNA was inserted into the NdeI/HindIII site of the pET28a(+) vector to construct the *E. coli* expression plasmid, pET28a(+):*hGUK1v2*. Next, to express *hGUK1v2* in mammalian cells, *hGUK1v2* cDNA was amplified by PCR using the EcoRI-hGUK1 Fw/hGUK1 Rv-NotI (*SI Appendix*, Table S2). The amplified cDNA was inserted into the EcoRI/NotI site of the pCAGIG vector (39) to construct the pCAGIG:*hGUK1v2*. These plasmids were amplified, purified, and sequenced as described above and then introduced into cultured cells.

Preparation of recombinant human GUK1 protein and kinase assay

For recombinant protein expression, *E. coli* Rosetta Gami B (DE3) cells (Merck) were transformed with pET28a(+):*hGUK1v2*. The transformed cells were cultured in 2 ml LB medium at 37°C for 16 h. Subsequently, the culture was inoculated into 100 ml LB medium and cultured at 37°C until reaching an OD600 of 0.5. Then, 1 mM IPTG was added and the culture was incubated at 28°C for 3 h before harvesting. The cells were suspended in 10 ml extraction buffer (50 mM Tris-HCl pH 7.5, 100 mM KCl, 10 mM $MgCl_2$, and 5% glycerol) supplemented with 1% protease inhibitor cocktail (Sigma-Aldrich P8465), sonicated, and the supernatant was collected after centrifugation at 10,000 × *g*. For affinity purification of His-tagged hGUK1 protein, 1 ml bed volume of Talon beads (Takara-Bio) was added to the supernatant. The mixture was incubated at 4°C for 1 h to allow binding. The beads were then packed into an open column. After washing with extraction buffer and extraction buffer supplemented with 10 mM imidazole, elution was performed using 10 ml of extraction buffer supplemented with 30 mM imidazole. The eluate was dialyzed four times against the extraction buffer to obtain the purified His-hGUK1 isoform b protein (hereafter, His-hGUK1). Purified His-hGUK1 was aliquoted, stored at -80°C, and used for enzyme activity assays. The protein concentration of His-hGUK1 was measured using XL-Bradford (SDS-PAGE) reagent with BSA as the standard. Purified His-hGUK1 protein was confirmed by SDS-PAGE separation and silver staining, along with *E. coli* whole extract before and after 3h of IPTG induction, and 100k × g supernatant from the post-induction extract.

His-hGUK1 protein activity assay

GMP/IMP phosphorylation activity was measured using purified His-hGUK1 protein according to the method described by Agarwal et al. (19). Briefly, the reaction of hGUK1 was observed as a decrease in the OD340 value, corresponding to the reduction in NADH via a coupled reaction of pyruvate kinase and lactate dehydrogenase using purine nucleoside diphosphate and phosphoenolpyruvate as substrates (*SI Appendix*, Fig. S9). The reaction was performed in a Nunc 96-well clear-bottom plate

(Thermo Fisher Scientific) with a reaction volume of 0.3 ml per well. The OD340 was measured over time at 30°C using a Tecan Infinite200Pro Plate reader (Tecan, Männedorf, Switzerland). The relationship between OD340 and the reaction products was determined by creating a calibration curve using ADP+GDP (product when GMP is the substrate) or ADP+IDP (product when IMP is the substrate) as standards in reactions with pyruvate kinase and lactate dehydrogenase. The initial velocity for each substrate concentration was determined from the time-dependent change in the amount of product obtained (0–20 s for the GMP substrate and 0–120 s for the IMP substrate). A Hanes-Woolf plot was created using Microsoft Excel (Microsoft, Redmond, WA, USA). K_m and V_{max} values were determined by a regression analysis using the least squares method. Furthermore, k_{cat} was calculated from the His-hGUK1 concentration (0.16 μM in the reaction mixture. To confirm IDP generation, the above reaction was performed without the addition of pyruvate kinase or lactate dehydrogenase. The reaction products were diluted with an equal volume of ice-cold buffer (50 mM EDTA, 40 mM t-butylamine, pH 6.8 with H_3PO_4) before filtration through an Ultrafiltration Spin Column 3 K (Pharma Foods). The filtrates were subjected to an HPLC analysis of IDP.

Preparation and analysis of *Itpa*$^{flox/flox}$/*Nes-Cre*/*Guk1* $^{+/-}$ mice

Guk1 KO mouse frozen sperm (C57BL/6NJ-Guk1em1(IMPC)J/Mmjax, JAX:037924, MMRRC:068325-JAX) was purchased from The Jackson Laboratory. The mutant *Guk1* allele (Guk1em1(IMPC)J) in this mouse was a KO allele generated using the CRISPR/Cas9 method. This mutation deleted ENSMUSE00000104732 (exon 4) and 332 bp of flanking intronic sequences, including the splice acceptor and donor. According to the Mutant Mouse Resource and Research Centers (MMRRC), this mutation is predicted to cause a change in the amino acid sequence after residue 72 and an early truncation 10 amino acids later. After *in vitro* fertilization using frozen sperm and C57BL/6J mouse oocytes, the embryos were transferred to surrogate ICR mice. Genomic DNA extracted from ear punch samples of the resulting offspring was subjected to typing PCR using a primer set, mGuk1 Fw/mGuk1 Rv, for KO and WT alleles (*SI Appendix*, Table S2), confirming a 103 bp band from the KO allele and a 532 bp band from the WT allele. *Guk1*$^{+/-}$ mice were crossed with *Itpa*$^{+/flox}$ /*Nes-Cre* mice to obtain *Itpa*$^{+/flox}$/*Nes-Cre*/*Guk1*$^{+/-}$ mice. These were then crossed with *Itpa*(flox/flox) mice to obtain *Itpa*$^{flox/flox}$ /*Nes-Cre*/*Guk1*$^{+/-}$ and *Itpa*$^{flox/flox}$/*Nes-Cre* mice. Typing PCR for the *Itpa*-flox allele and the *Nes-Cre* transgene was performed as described by Koga et al. (13). Some mice underwent body weight measurements from postnatal day 14 (P14) to P30, and their lifespans were assessed up to P60. Weaning was performed at P30. For tissue collection, the mice were euthanized under deep anesthesia by ice-cold saline perfusion at P17 or P18. Cerebral cortex tissues were immediately harvested, frozen in liquid nitrogen, stored at -80°C, and subsequently used for protein and RNA extraction. All animals were maintained in a temperature-controlled (22°C ± 2°C, 55% ± 5% humidity), specific pathogen-free room with a 12-h light/12-h dark cycle. All animal

experimental procedures were reviewed and approved by the Animal Care and Use Committee of Kyushu University (approval number: A24-384-0).

Statistical analysis

Statistical significance was assessed using the JMP Student's Edition software program (SAS Institute Japan Ltd., Tokyo, Japan). Welch's *t* test and Tukey's HSD test were used to compare two groups and multiple comparisons with parametric data, respectively. Normality tests were performed using the Shapiro-Wilk test. Parametric data are shown as dot plots and bar graphs with error bars (standard deviations). The Wilcoxon signed-rank test or 2-way analysis of variance (ANOVA) after aligned rank transform was used for non-parametric data. Non-parametric data are shown as dot plots and box plots (center line, median; box limits, upper and lower quartiles; whiskers, 1.5 × interquartile range). Pearson's correlation analysis was used to examine the relationships between the two variables. Pearson's χ^2 test was used to analyze the ratio of genotypes in the newborn mice. Mouse survival was compared using the log-rank test.

Data, Materials, and Software Availability. Study data are included in the article and/or *SI Appendix*.

Acknowledgements

We thank Masato Tanaka from the Laboratory of Embryonic and Genetic Engineering and Ryo Ugawa from the Laboratory for Research Support, Medical Institute of Bioregulation, Kyushu University for their technical support. We appreciate the technical assistance from The Research Support Center, Research Center for Human Disease Modeling, Kyushu University Graduate School of Medical Sciences, which is partially supported by the Mitsuaki Shiraishi Fund for Basic Medical Research. We thank Drs. Kunihiko Sakumi, Nona Abolhassan, and Yoriko Akimoto for their technical advice on the HPLC analysis, and Drs. Mizuki Ohno and Sato Yoshidomi for their support in shRNA screening and western blotting, respectively. We thank Japan Medical Communication (https://www.japan-mc.co.jp/) for editing this manuscript. This work was supported in part by grants from the Japan Society for the Promotion of Science (grant numbers 18K06960 and 21K06869 to DT and 17H01391 to YN) and grants for MIB, Kyushu University, by the MEXT Cooperative Research Project Program, Medical Research Center Initiative for High Depth Omics, and Coalition of Universities for Research Excellence Program (CURE, grant number JPMXP1323015486).

Author contributions: D.T. designed research; D.T. and Y.T. performed research; D.T. analyzed data; and D.T. and Y.N. wrote the paper.

Conflict of interest

The authors declare no conflicts of interest in association with the present study.

References

1. N. E. Burgis, R. P. Cunningham, Substrate specificity of RdgB protein, a deoxyribonucleoside triphosphate pyrophosphohydrolase. *J. Biol. Chem.* **282**, 3531-3538 (2007).
2. S. Lin *et al.*, Cloning, expression, and characterization of a human inosine triphosphate pyrophosphatase encoded by the itpa gene. *J. Biol. Chem.* **276**, 18695-18701 (2001).
3. N. E. Burgis, A disease spectrum for ITPA variation: advances in biochemical and clinical research. *J. Biomed. Sci.* **23**, 73 (2016).
4. H. P. Jiang *et al.*, Modified nucleoside triphosphates exist in mammals. *Chem. Sci.* **9**, 4160-4167 (2018).
5. K. Sakumi *et al.*, ITPA protein, an enzyme that eliminates deaminated purine nucleoside triphosphates in cells. *Mutat. Res.* **703**, 43-50 (2010).
6. J. H. Schroader, M. T. Handley, K. Reddy, Inosine triphosphate pyrophosphatase: A guardian of the cellular nucleotide pool and potential mediator of RNA function. *Wiley Interdiscip. Rev. RNA* **14**, e1790 (2023).
7. N. Abolhassani *et al.*, NUDT16 and ITPA play a dual protective role in maintaining chromosome stability and cell growth by eliminating dIDP/IDP and dITP/ITP from nucleotide pools in mammals. *Nucleic Acids Res.* **38**, 2891-2903 (2010).
8. M. Behmanesh *et al.*, ITPase-deficient mice show growth retardation and die before weaning. *Cell Death Differ.* **16**, 1315-1322 (2009).
9. K. Taghizadeh *et al.*, Quantification of DNA damage products resulting from deamination, oxidation and reaction with products of lipid peroxidation by liquid chromatography isotope dilution tandem mass spectrometry. *Nat. Protoc.* **3**, 1287-1298 (2008).
10. S. H. Kevelam *et al.*, Recessive ITPA mutations cause an early infantile encephalopathy. *Ann. Neurol.* **78**, 649-658 (2015).
11. M. Scala *et al.*, Clinico-radiological features, molecular spectrum, and identification of prognostic factors in developmental and epileptic encephalopathy due to inosine triphosphate pyrophosphatase (ITPase) deficiency. *Hum. Mutat.* **43**, 403-419 (2022).
12. K. Burton, H. White, J. Sleep, Kinetics of muscle contraction and actomyosin NTP hydrolysis from rabbit using a series of metal-nucleotide substrates. *J. Physiol.* **563**, 689-711 (2005).
13. Y. Koga *et al.*, Neural stem cell-specific ITPA deficiency causes neural depolarization and epilepsy. *JCI Insight* **5** (2020).

14. Y. Hitomi *et al.*, Inosine triphosphate protects against ribavirin-induced adenosine triphosphate loss by adenylosuccinate synthase function. *Gastroenterology* **140**, 1314-1321 (2011).
15. K. Takeuchi *et al.*, The GTP responsiveness of PI5P4Kbeta evolved from a compromised trade-off between activity and specificity. *Structure* **30**, 886-899 e884 (2022).
16. J. H. Schroader *et al.*, Disease-associated inosine misincorporation into RNA hinders translation. *Nucleic Acids Res.* **50**, 9306-9318 (2022).
17. J. R. Averill, H. Jung, Mutagenic incorporation of inosine into DNA via T:I mismatch formation by human DNA polymerase eta (poleta). *Biochem. J.* **480**, 649-664 (2023).
18. B. Pang *et al.*, Defects in purine nucleotide metabolism lead to substantial incorporation of xanthine and hypoxanthine into DNA and RNA. *Proc. Natl. Acad. Sci. U.S.A.* **109**, 2319-2324 (2012).
19. R. P. Agarwal, E. M. Scholar, K. C. Agarwal, R. E. Parks, Jr., Identification and isolation on a large scale of guanylate kinase from human erythrocytes. Effects of monophosphate nucleotides of purine analogs. *Biochem. Pharmacol.* **20**, 1341-1354 (1971).
20. H. Ren *et al.*, The crystal structure of human adenylate kinase 6: An adenylate kinase localized to the cell nucleus. *Proc. Natl. Acad. Sci. U.S.A* **102**, 303-308 (2005).
21. M. Boissan, U. Schlattner, M. L. Lacombe, The NDPK/NME superfamily: state of the art. *Lab. Invest.* **98**, 164-174 (2018).
22. I. Lascu, P. Gonin, The catalytic mechanism of nucleoside diphosphate kinases. *J. Bioenerg. Biomembr.* **32**, 237-246 (2000).
23. Q. Lu, M. Inouye, Adenylate kinase complements nucleoside diphosphate kinase deficiency in nucleotide metabolism. *Proc. Natl. Acad. Sci. U.S.A.* **93**, 5720-5725 (1996).
24. S. Schaertl, M. Konrad, M. A. Geeves, Substrate specificity of human nucleoside-diphosphate kinase revealed by transient kinetic analysis. *J. Biol. Chem.* **273**, 5662-5669 (1998).
25. A. E. Vidal *et al.*, Inosine triphosphate pyrophosphatase from Trypanosoma brucei cleanses cytosolic pools from deaminated nucleotides. *Sci. Rep.* **12**, 6408 (2022).
26. T. Borza, C. V. Iancu, E. Pike, R. B. Honzatko, H. J. Fromm, Variations in the response of mouse isozymes of adenylosuccinate synthetase to inhibitors of physiological relevance. *J. Biol. Chem.* **278**, 6673-6679 (2003).
27. Y. Matsuda, H. Ogawa, S. Fukutome, H. Shiraki, H. Nakagawa, Adenylosuccinate synthetase in rat liver: the existence of two types and their regulatory roles. *Biochem. Biophys. Res. Commun.* **78**, 766-771 (1977).
28. W. A. Brady, M. S. Kokoris, M. Fitzgibbon, M. E. Black, Cloning, characterization, and modeling of mouse and human guanylate kinases. *J. Biol. Chem.* **271**, 16734-16740 (1996).

29. A. Hidalgo-Gutierrez *et al.*, Guanylate Kinase 1 Deficiency: A Novel and Potentially Treatable Mitochondrial DNA Depletion/Deletions Disease. *Ann. Neurol.* **96**, 1209-1224 (2024).
30. P. C. Dedon, S. R. Tannenbaum, Reactive nitrogen species in the chemical biology of inflammation. *Arch Biochem. Biophys.* **423**, 12-22 (2004).
31. E. G. Prestwich *et al.*, Increased levels of inosine in a mouse model of inflammation. *Chem. Res. Toxicol.* **26**, 538-546 (2013).
32. H. Straube *et al.*, An inosine triphosphate pyrophosphatase safeguards plant nucleic acids from aberrant purine nucleotides. *New Phytol.* **237**, 1759-1775 (2023).
33. Y. Hellsten, E. A. Richter, B. Kiens, J. Bangsbo, AMP deamination and purine exchange in human skeletal muscle during and after intense exercise. *J. Physiol.* **520 Pt 3**, 909-920 (1999).
34. H. Zhao *et al.*, Quantitative analysis of purine nucleotides indicates that purinosomes increase de novo purine biosynthesis. *J Biol Chem* **290**, 6705-6713 (2015).
35. J. L. Schneider *et al.*, GUK1 activation is a metabolic liability in lung cancer. *Cell* **188**, 1248-1264 e1223 (2025).
36. K. Wolfe *et al.*, Dynamic compartmentalization of purine nucleotide metabolic enzymes at leading edge in highly motile renal cell carcinoma. *Biochem. Biophys. Res. Commun.* **516**, 50-56 (2019).
37. P. G. Plagemann, R. M. Wohlhueter, M. Kraupp, Adenine nucleotide metabolism and nucleoside transport in human erythrocytes under ATP depletion conditions. *Biochim. Biophys. Acta.* **817**, 51-60 (1985).
38. E. Iwama *et al.*, Cancer-related PRUNE2 protein is associated with nucleotides and is highly expressed in mature nerve tissues. *J. Mol. Neurosci.* **44**, 103-114 (2011).
39. T. Matsuda, C. L. Cepko, Electroporation and RNA interference in the rodent retina in vivo and in vitro. *Proc. Natl. Acad. Sci. U.S.A.* **101**, 16-22 (2004).

Figure legends

Fig. 1.

Screening of genes that are indispensable for ITP biosynthesis.

(A) Western blotting of ITPA protein in Neuro2a *Itpa* knockout (KO) clone #1-16-9 and three other incomplete KO clones. Ten micrograms of protein of whole cell extract was loaded in each lane. Arrowhead indicates the mouse ITPA signal. Ponceau-S staining of the membrane was used as a loading control. These images are shown in *SI Appendix*, Fig. S3. (B) HMGA (hypoxanthine, mycophenolic acid, guanosine, and adenosine) treatment increases intracellular inosine monophosphate (IMP) levels and accelerates inosine triphosphate (ITP) biosynthesis. H: Hypoxanthine (1000 μM), converted to IMP by hypoxanthine phosphoribosyl transferase 1. M: Mycophenolic acid (10 μM), which inhibits IMP dehydrogenase 1 and 2. G: Guanosine (250 μM), which is converted to GMP and compensates for reduced guanosine monophosphate (GMP) synthesis by mycophenolic acid. A: Adenosine (250 μM), which is converted to adenosine monophosphate (AMP) and inhibits adenylosuccinate synthetases 1 and 2. HMGA (hypoxanthine, mycophenolic acid, guanosine, and adenosine) treatment is expected to cause accumulation of IMP and ITP. (C) ITPA-deficient cell-specific cell growth suppression following HMGA treatment. Neuro2a cells (N2a) and Neuro2a *Itpa*-KO clone #1-16-9 (KO) were cultured for four days with HMGA or other combinations of supplements. Cell proliferation was analyzed using a cell counting kit-8 and is shown as a percentage ratio to those of the control without the supplements. Mean ± SD values (n = 9) are shown. The statistical analysis was performed using the Tukey-Kramer HSD post-hoc multiple comparison test, and bars without the same letter were significantly different. (D) Screening procedure. Neuro2a *Itpa*-KO #1-16-9 cells were transduced with a mouse shRNA lentiviral library and cultured for four weeks with HMGA. The frequency of each siRNA coding sequence in the genomic DNA was analyzed and compared between cells harvested before and after HMGA treatment.

Fig. 2.

Correlation of the GUK1 expression and the inosine level in RNA in mouse Neuro2a *Itpa*-knockout (KO) cell-derived *Guk1*-knockdown (KD) clones.

(A) Western blotting of mouse GUK1 protein in Neuro2a *Itpa*-KO/*Guk1*-KD clones #11 and #13. Neuro2a and Neuro2a *Itpa*-KO clone #1-16-9 (*Itpa*-KO) were used as the controls. Ten micrograms of protein of whole cell extract was loaded in each lane. The two arrowheads indicate mouse GUK1 signals. Ponceau-S staining of the membrane was used as a loading control. These images are shown in *SI Appendix*, Fig. S3. (B) Proliferation of Neuro2a, *Itpa*-KO, *Itpa*-KO/*Guk1*-KD clone #11, and *Itpa*-KO/*Guk1*-KD clone #13, with or without HMGA (hypoxanthine, mycophenolic acid, guanosine, and adenosine) treatment. The cells were cultured for 4 days, and their proliferation was analyzed using a cell counting kit-8. The mean ± SD of relative % values to the mean of control without HMGA are shown for each cell (n = 5). (C) Inosine content per 10^6 guanosine molecules in RNA from Neuro2a, *Itpa*-KO, Neuro2a *Itpa*-KO/*Guk1*-KD clone #11, and clone #13 with or without HMGA treatment (n = 7). The inosine and guanosine content in the RNA was quantified using HPLC. (D) Positive correlation between inosine content in RNA and *Guk1* mRNA expression levels in 11 clones of Neuro2a *Itpa*-KO/*Guk1*-KD cells, including clones #11 and #13, and control (*Itpa*-KO). The mean values of the inosine content (n = 7 for #11, #13, and control; n = 2 for other clones) and *Guk1* mRNA levels (n = 2) of 12 clones are shown as a scatter plot graph. The original data are listed in *SI Appendix*, Table S3. Pearson's correlation coefficient between the inosine content in RNA and the *Guk1* mRNA level was 0.979529. Red and green show the regression line and the 95% confidence ellipse, respectively. (E) Neuro2a *Itpa*-KO/*Guk1*-KD clone #13 cells were transiently transfected with the human GUK1 expression plasmid (pCAGIG:hGUK1v2) or control vector (pCAGIG) and cultured for 3 days. Mean ± SD values of inosine content in RNA (left, n = 5) and a result of western blotting with anti-GUK1 (right, 10 μg total protein/lane) are shown. Ponceau S staining of the membrane is shown as a loading control (right). In (B) and (C), a statistical analysis was performed using the Tukey-Kramer HSD test, and bars without the same letter were significantly different. In (E) a statistical analysis was performed using Welch's t-test.

Fig. 3.

Enzyme activity of recombinant human GUK1 protein.

(A) The expression and purification of human GUK1 isoform b protein with an N-terminal His-tag (His-hGUK1). Whole cell extracts from 10µl *E. coli* culture before and after 3h of IPTG induction, and 10 µl of purified protein solution were separated by SDS-PAGE and subjected to silver staining. Arrowhead indicates the recombinant His-hGUK1 protein. The image of the entire gel is shown in *SI Appendix*, Fig. S8. (B) Hanes-Woolf plots of the phosphorylation activity of His-hGUK1 protein using ATP plus guanosine monophosphate (GMP) or inosine monophosphate (IMP) as substrates. His-hGUK1 activity is coupled with pyruvate kinase and lactate dehydrogenase activities. The coupled activity was monitored by measuring OD340 of NADH. (C) High-performance liquid chromatography chromatograms of His-hGUK1 products. His-hGUK1 was incubated with 4 mM adenosine triphosphate (ATP) and 5mM inosine monophosphate (IMP) without pyruvate or lactate dehydrogenase, to confirm its products by HPLC. (D) UV spectra of peak 1, peak 2, adenosine monophosphate (AMP) standard peak, and IDP standard peak in (C).

Fig. 4.

Effects of *Guk1* haplo-insufficiency on ITPA deficient and proficient mice.

(A) Western blots of ITPA or GUK1 protein in cerebral cortex of *Itpa*$^{flox/flox}$ mice (control), *Itpa*$^{flox/flox}$/*Nes-Cre* mice (*Itpa* cKO), and *Itpa*$^{flox/flox}$/*Nes-Cre*/*Guk1*$^{+/-}$ mice (*Itpa* cKO/*Guk1*$^{+/-}$). Ten micrograms of cortex extract protein derived from three female mice was loaded for each genotype. ITPA and GUK1 proteins were detected using western blotting and quantified using a standard curve. The standard curve was prepared using control lanes and normalized by the intensity of Ponceau-S staining of each lane as a loading control. The mean relative band signal intensities and standard deviations are shown in the band images. Signals on lanes for the standard curve and Ponceau S staining image are shown in *SI Appendix*, Fig. S8. (B) Body weights of the ITPA-deficient mice. Body weights of the *Itpa* cKO mice (control, 18 females and 11 males) and *Itpa* cKO/*Guk1*$^{+/-}$ mice (11 females and 14 males) at postnatal day 17 (P17) are shown. The effect of *Guk1* genotype on the body weight of ITPA-deficient mice was not significant ($p = 0.2884$). (C) Survival curves of *Itpa* cKO mice (13 females and 8 males) and *Itpa* cKO/*Guk1*$^{+/-}$ mice (9 females and 10 males). The difference between the two genotypes was significant ($p < 0.0001$, log-rank test). (D) Inosine content per 10^6 guanosine in the RNA of *Itpa* cKO mice and *Itpa* cKO/*Guk1*$^{+/-}$ mice (n = 8, 4 females and 4 males) at P17 and P18. The difference between them was significant ($p = 0.0008$, Wilcoxon signed-rank test). (E) Body weights of the ITPA-proficient mice. The body weights of *Guk1*$^{+/+}$ and *Guk1*$^{+/-}$ ITPA-proficient mice at P14 are shown (n = 10–22). The effects of *Guk1* genotype ($p = 0.0362$) and sex ($p = 0.7939$) were analyzed using a 2-way analysis of variance after aligned rank transform ($p = 0.1863$, interaction; $p = 0.6857$).

Table legends

Table 1. The genes targeted by the multiple selected shRNAs
The shRNAs which could rescue the cells treated with HMGA were selected in the analysis step 1 and 2 in Figure 1D. Only three genes were targeted by the multiple selected shRNAs.

Table 2. Kinetic parameters of His-hGUK1
Kinetic parameters of His-hGUK1 with GMP or IMP were determined using Hanes-Woolf plots in Fig. 3B.

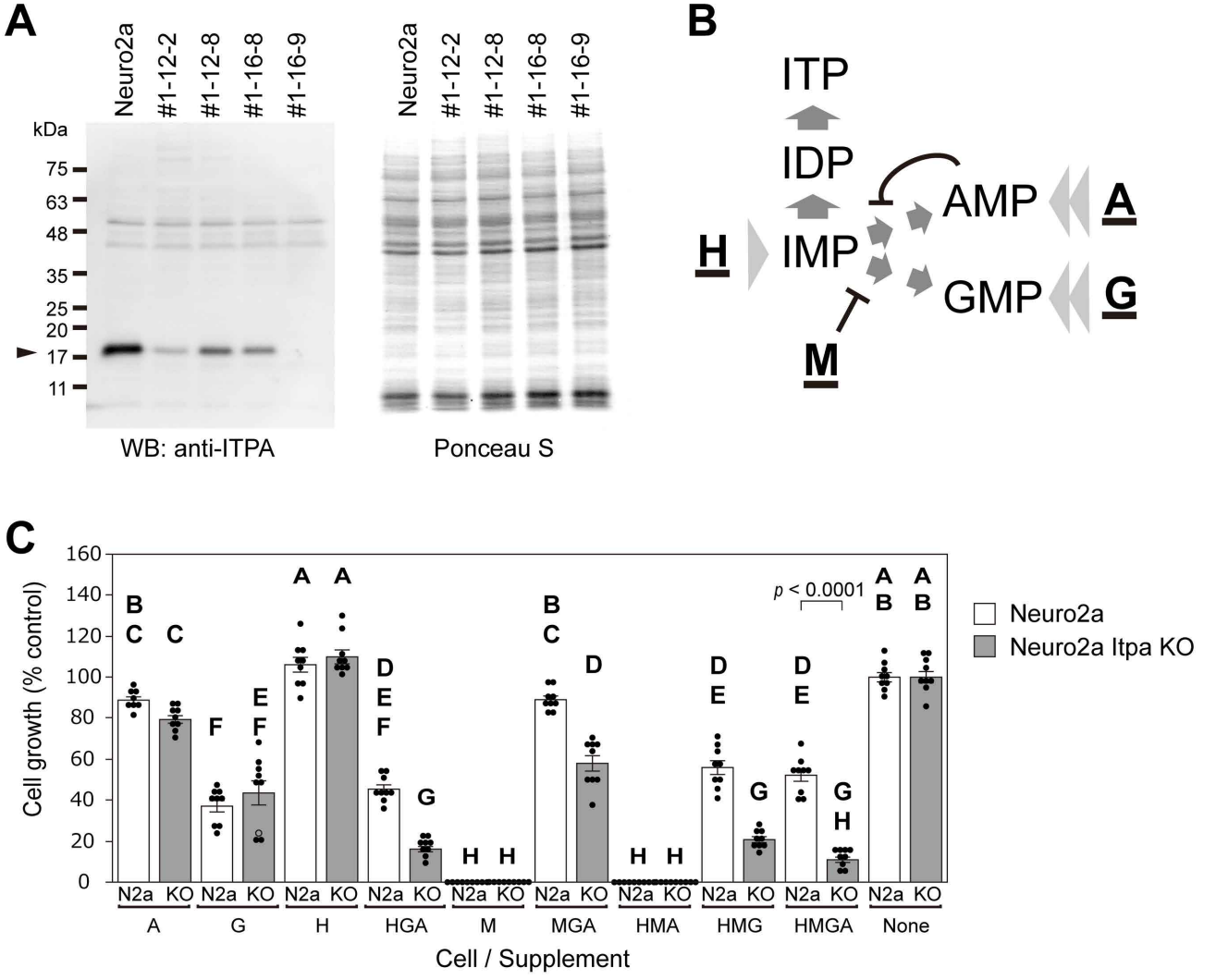
A
Neuro2a
#1-12-2
#1-12-8
#1-16-8
#1-16-9
kDa
75
63
48
35
25
20
17
11
WB: anti-ITPA
Ponceau S
B
ITP
IDP
IMP
AMP
GMP
H
A
G
M
C
Cell growth (% control)
p < 0.0001
Neuro2a
Neuro2a Itpa KO
N2a
KO
A
G
H
HGA
M
MGA
HMA
HMG
HMGA
None
Cell / Supplement
D
Transduction of cells with mouse shRNA viral library
4 weeks culture with HMGA
Harvest allequotes of the cells before and after the HMGA selection.
Analysis steps
1. Check frequency of each shRNA code in total genomic DNA before and after HMGA treatment (4 weeks).
2. Selection of shRNA codes whose frequencies increased 10 fold during the HMGA treatment.
3. Selection of mouse genes that are targeted by the multiple shRNA codes selected in step 2.

Fig. 1

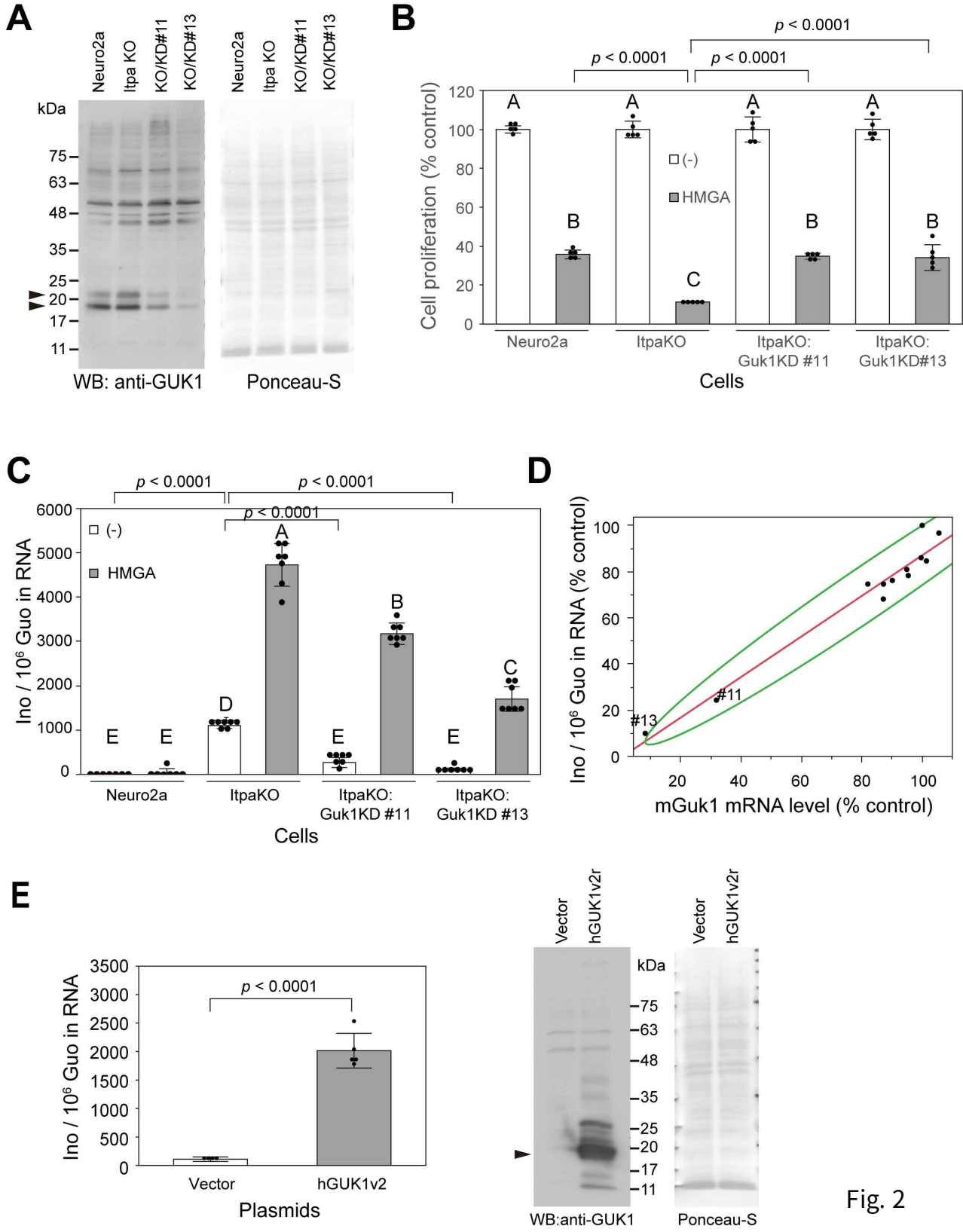
A
Neuro2a
Itpa KO
KO/KD#11
KO/KD#13
kDa
75
63
48
35
25
20
17
11
WB: anti-GUK1
Ponceau-S
B
p < 0.0001
p < 0.0001
p < 0.0001
Cell proliferation (% control)
(-)
HMGA
Neuro2a
ItpaKO
ItpaKO: Guk1KD #11
ItpaKO: Guk1KD#13
Cells
C
p < 0.0001
p < 0.0001
p < 0.0001
Ino / 10⁶ Guo in RNA
(-)
HMGA
Neuro2a
ItpaKO
ItpaKO: Guk1KD #11
ItpaKO: Guk1KD #13
Cells
D
Ino / 10⁶ Guo in RNA (% control)
mGuk1 mRNA level (% control)
#13
#11
E
p < 0.0001
Ino / 10⁶ Guo in RNA
Vector
hGUK1v2
Plasmids
Vector
hGUK1v2r
kDa
WB:anti-GUK1
Ponceau-S

Fig. 2

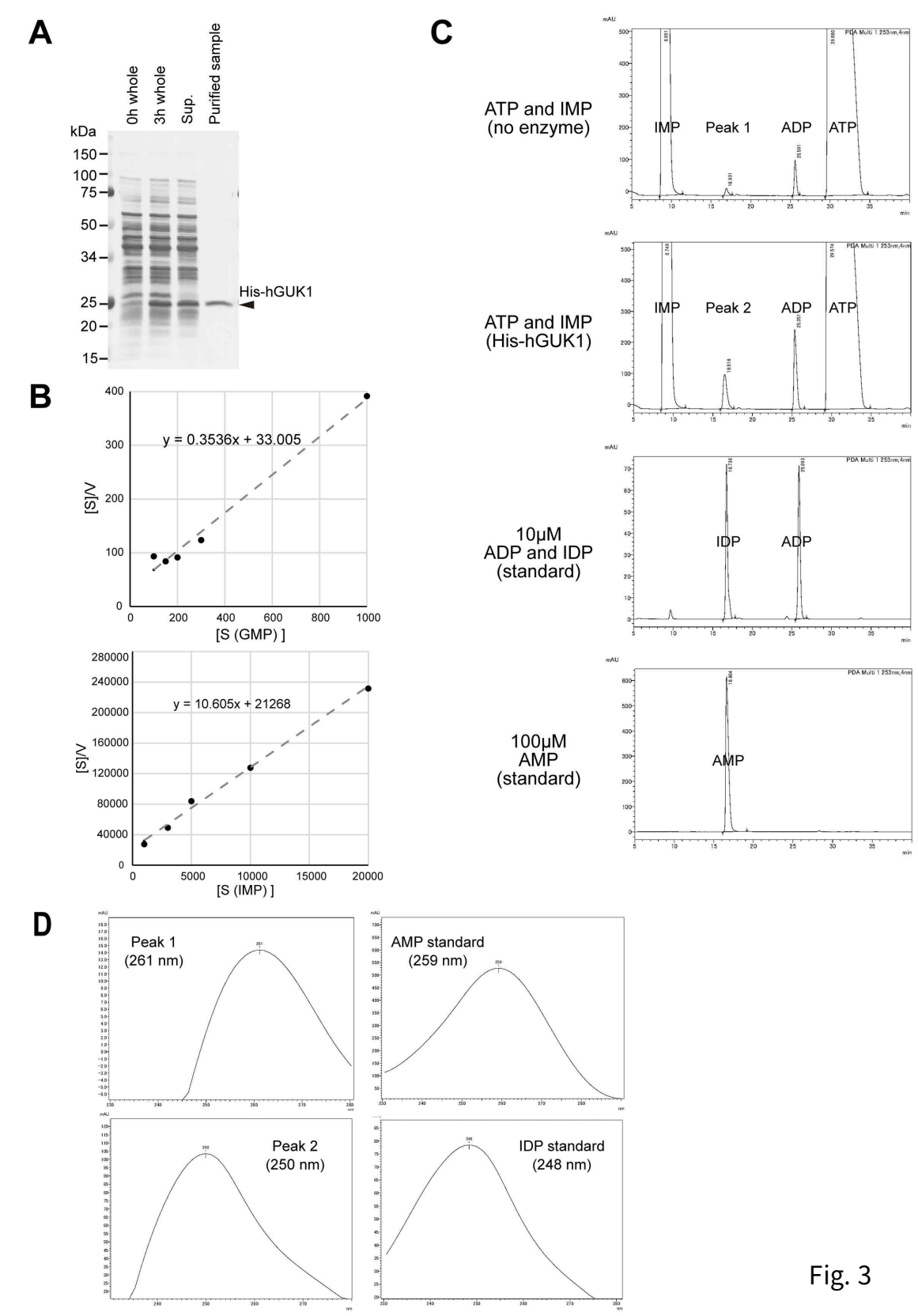
A
0h whole
3h whole
Sup.
Purified sample
kDa
150
100
75
50
34
25
20
15
His-hGUK1
B
y = 0.3536x + 33.005
[S]/V
[S (GMP)]
y = 10.605x + 21268
[S]/V
[S (IMP)]
C
ATP and IMP
(no enzyme)
IMP
Peak 1
ADP
ATP
ATP and IMP
(His-hGUK1)
IMP
Peak 2
ADP
ATP
10μM
ADP and IDP
(standard)
IDP
ADP
100μM
AMP
(standard)
AMP
D
Peak 1
(261 nm)
AMP standard
(259 nm)
Peak 2
(250 nm)
IDP standard
(248 nm)

Fig. 3

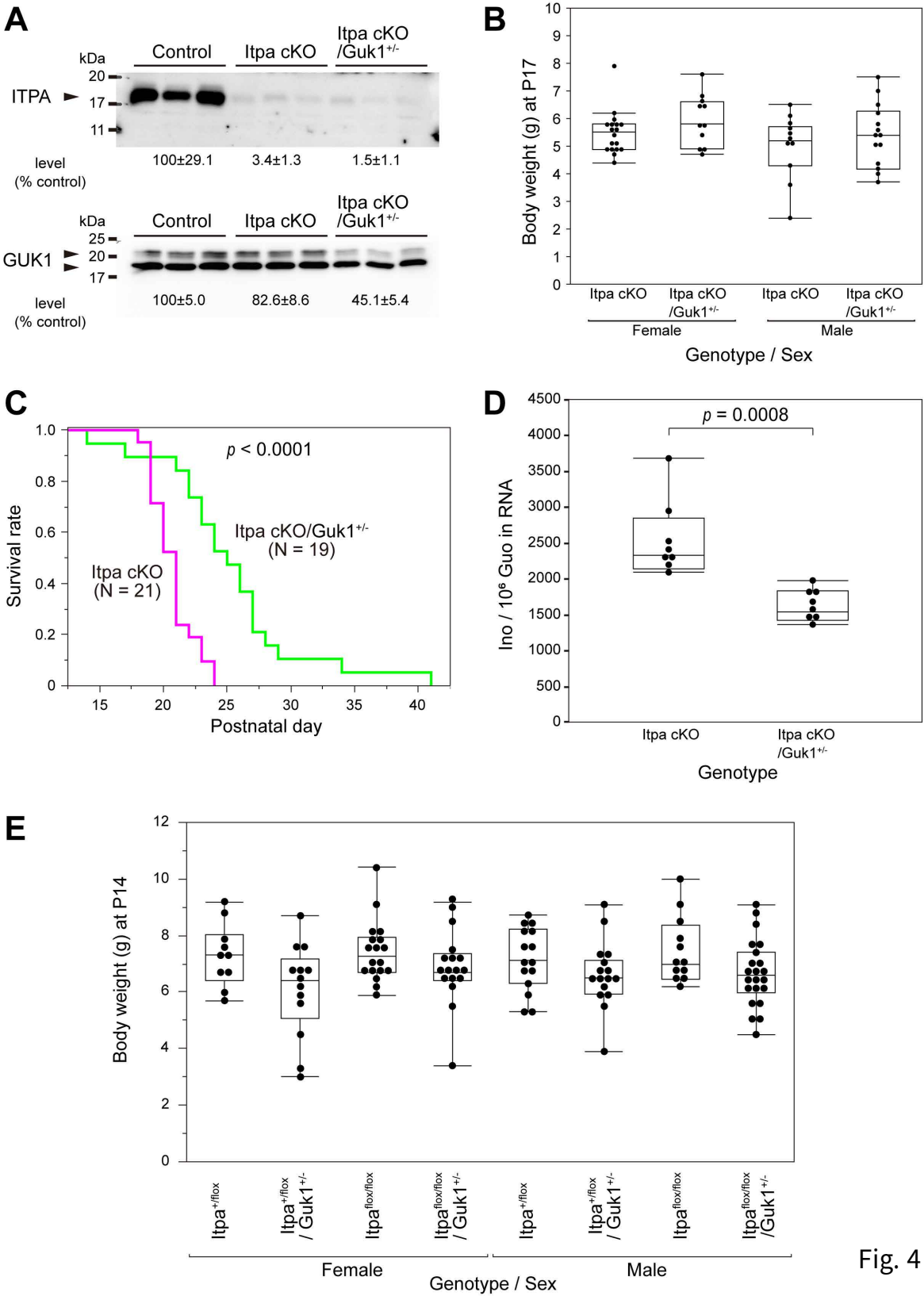
A
kDa
Control
Itpa cKO
Itpa cKO /Guk1+/-
ITPA
20
17
11
level (% control)
100±29.1
3.4±1.3
1.5±1.1
GUK1
25
20
17
100±5.0
82.6±8.6
45.1±5.4
B
Body weight (g) at P17
Itpa cKO
Itpa cKO /Guk1+/-
Female
Male
Genotype / Sex
C
Survival rate
p < 0.0001
Itpa cKO/Guk1+/- (N = 19)
Itpa cKO (N = 21)
Postnatal day
D
p = 0.0008
Ino / 10^6 Guo in RNA
Genotype
E
Body weight (g) at P14
Itpa+/flox
Itpa+/flox / Guk1+/-
Itpaflox/flox
Itpaflox/flox / Guk1+/-
Female
Male
Genotype / Sex

Fig. 4

Table 1. The genes targeted by the multiple selected shRNAs

Target mouse gene	Number of the selected shRNAs
Guk1	4 shRNAs in library module #2
Lamp5	2 shRNAs in library module #2
Raf1	2 shRNAs in library module #1

Table 2. Kinetic parameters of His-hGUK1

Substrate	K_m (μM)	V_{max} (μM/sec)	k_{cat} (1/sec)
GMP	93.3	2.83	17.6
IMP	2005	0.094	0.59

Supporting Information for

Guanylate kinase 1 is an enzyme responsible for inosine accumulation in RNA of mammalian cells deficient in inosine triphosphatase

Daisuke Tsuchimoto[a,b,1], Yuka Takiguchi[b], and Yusaku Nakabeppu[b]
[a]Division of Neurofunctional Genomics, Advanced Research Initiative, Research Promotion Unit, Medical Institute of Bioregulation, Kyushu University, Fukuoka, 8128582, Japan
[b]Division of Neurofunctional Genomics, Department of Immunobiology and Neuroscience, Medical Institute of Bioregulation, Kyushu University, Fukuoka, 8128582, Japan

[1]Corresponding author: Daisuke Tsuchimoto
Email: daisuke_nfg@kyudai.jp

This PDF file includes:
Figure S1-S10
Table S1-S5

Other supporting materials include the following:
Dataset S1, S2, S3

Supporting Information Text

Nucleosides, nucleotides, and synthetic Oligo DNA

IMP, inosine diphosphate (IDP), inosine (Ino), guanosine (Guo), adenosine (Ado), and guanosine monophosphate (GMP) were purchased from Sigma-Aldrich (St. Louis, MO); guanosine diphosphate (GDP) and adenosine diphosphate (ADP) were purchased from Yamasa (Choshi, Chiba, Japan); and ATP and hypoxanthine were purchased from Thermo Fisher Scientific (Waltham, MA). All oligonucleotides (*SI Appendix*, Table S2) were synthesized by Sigma-Aldrich.

Cell culture and plasmid transfection

All cultured cells were maintained in Dulbecco's modified Eagle's medium with high glucose (Fujifilm, Tokyo, Japan) supplemented with 10% fetal bovine serum (PAA Laboratories GmbH, Pasching, Austria) and 1% penicillin-streptomycin (final 100 units penicillin/ml, 100 μg streptomycin/ml, Fisher Scientific) at 37°C under 5% CO_2. The mouse neuroblastoma-derived cell line Neuro2a (ATCC No. CCL-131) was purchased from the American Type Culture Collection (ATCC, Manassas, VA, USA). For introduction into cultured cells, plasmid DNAs was amplified in *Escherichia coli* DH5alpha cells (Toyobo, Osaka, Japan). DNA was extracted and purified using a Genopure Plasmid Maxi Kit (Sigma-Aldrich). Endotoxins were removed using a MiraCLEAN Endotoxin Removal Kit (Takara Bio, Kyoto, Japan). Their sequences were confirmed by Sanger sequencing, and the plasmids were introduced into cultured cells using Effectene reagent (Qiagen).

Establishment of Neuro2a *Itpa*-KO clone

The *Itpa*-KO clone derived from Neuro2a cells was established using the CRISPR/Cas9 method to cleave the sequence within exon 4. Specifically, guide RNA sequences targeting the Ex4_1 sequence (*SI Appendix*, Table S2) within exon 4 of the *Itpa* gene were designed using CRISPR Direct software program (https://crispr.dbcls.jp) (1). Oligo DNA pairs Ex4_1 sense/Ex4_1 anti (*SI Appendix*, Table S2) were annealed and inserted into the BbsI site of pSpCas9(BB)-2A-Puro (PX459) (Addgene ID: 48139) (2) to construct pX459v2:mItpa Ex4_1. This plasmid was introduced into Neuro2a cells using the above-described method. Temporary selection was performed using 2.0 μg/ml puromycin from 24 to 48 h post-transfection. The cells were then diluted and replated to form colonies, and individual colonies were selected for cloning. The target site within the genomic DNA of each clone was amplified by PCR using the primer sets Ex4_target seq Fw3/Ex4_target seq Rv3 and Ex4_target seq Fw4/Ex4_target seq Rv4 (*SI Appendix*, Table S2). The nucleotide sequence was analyzed by direct Sanger sequencing using Primer Ex4_ target-seq Fw3. Chromatogram data from Sanger sequencing were analyzed using the TIDE software program (http://shinyapps.datacurators.nl/tide) (3) to confirm

the wild-type (WT) allele and insertion/deletion alleles. For clones in which both insertion/deletion alleles and the WT allele were confirmed, the plasmid was reintroduced, cloning was performed, and a TIDE analysis of the target site was conducted. For clones in which the TIDE analysis confirmed the loss of the WT sequence, loss of the ITPA protein expression was confirmed by western blotting using anti-ITPA antisera.

Western blotting of ITPA and GUK1 proteins

Frozen mouse tissue samples and cultured cells were homogenized in sodium dodecyl sulfate (SDS) sample buffer (62.5 mM Tris-HCl pH 6.8, 2% SDS, 5% glycerol, 2% 2-mercaptoethanol, and 0.005% bromophenol blue) using a Potter Teflon homogenizer (Thomas Scientific, Swedesboro, New Jersey, USA) at 4°C. Protein concentrations were analyzed using XL-Bradford (SDS-PAGE) reagent (Pharma Foods, Kyoto, Japan) with bovine serum albumin (BSA) (Thermo Fisher Scientific) as the standard protein. Denatured protein samples (5 or 10 μg total protein/lane) were separated using SDS-PAGE and transferred onto an Immobilon-P PVDF membrane (Merck, Darmstadt, Germany). The membranes were stained with Ponceau S. Ponceau S staining images were captured using a GT-X900 scanner (EPSON, Tokyo, Japan). Membranes were blocked by incubation for 1 h at room temperature in Tris-buffered saline with Tween-20 (TBST; 10 mM Tris-HCl pH 7.5, 0.9% NaCl, 0.1% Tween-20) containing 5% non-fat dried milk (MegMilk Snow Brand, Tokyo, Japan). The membranes were incubated in TBST containing anti-ITPA rabbit antiserum (4) (1:1000 dilution) or an anti-GUK1 mouse monoclonal antibody (Proteintech, Rosemont, IL, USA) (1:2000 dilution) for 16 h at 4°C with gentle shaking. After washing with TBST, the membranes were incubated in TBST containing anti-rabbit IgG HRP-linked goat or anti-mouse IgG HRP-linked goat antibodies (1:3000 dilution; Cell Signaling Technology, Danvers, MA, USA) for 1 h at room temperature. After washing with TBST, the antibodies on the blots were detected using the chemiluminescence method with Western BLoT Quant HRP Substrate (Takara-Bio). Digitized images were obtained using an AE-9300 Ez-Capture MG system (ATTO, Tokyo, Japan). The signal intensity of each band in the western blotting or signal intensity in each lane on Ponceau-S staining was quantified using the CS analyzer image analysis software program (ATTO, Tokyo, Japan).

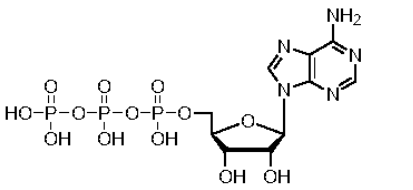

ATP

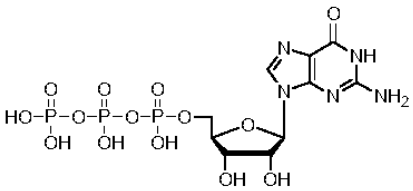

GTP

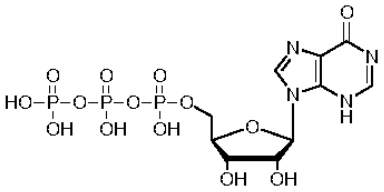

ITP

Figure S1. Structures of canonical and non-canonical purine nucleoside triphosphates.

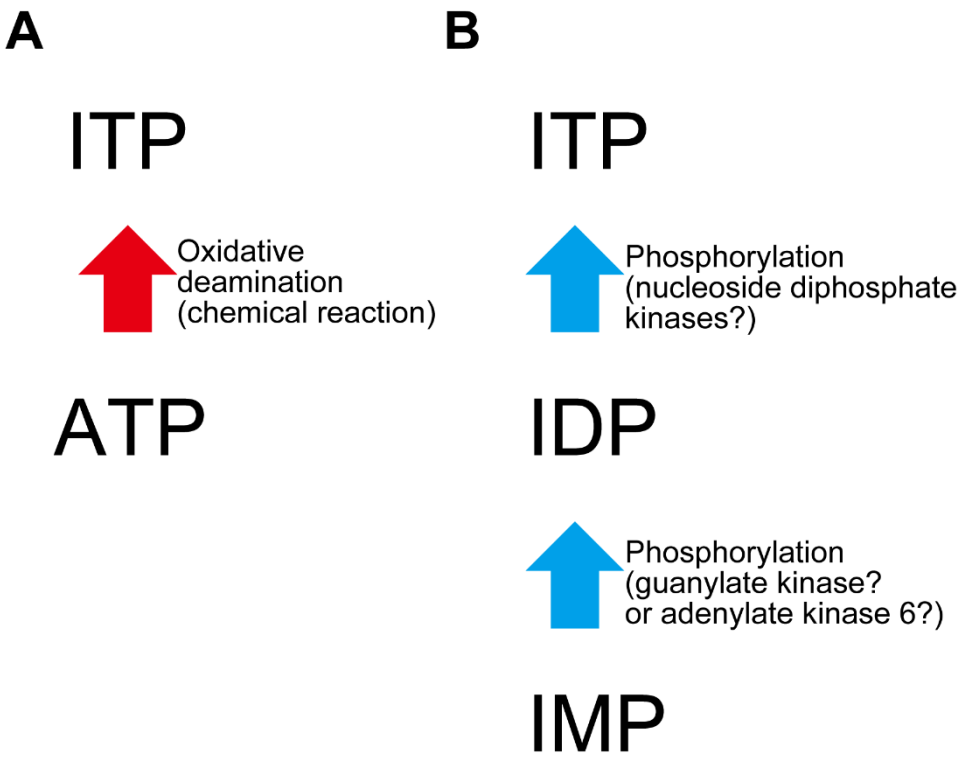

Figure S2. Previous two hypotheses of biosynthesis of inosine triphosphate (ITP). (A). Oxidative deamination at the C6 site of adenosine in adenosine triphosphate (ATP) occurs via a chemical reaction. (B). Two-step phosphorylation of inosine monophosphate (IMP) (5). The first step is the phosphorylation of IMP. Guanylate kinase and adenylate kinase 6 are candidates for the enzyme responsible for the first step (6,7). The second step is the phosphorylation of IDP. Nucleoside diphosphate kinases, which have a relatively low substrate specificity in base moiety (8-10), are thought to catalyze this step.

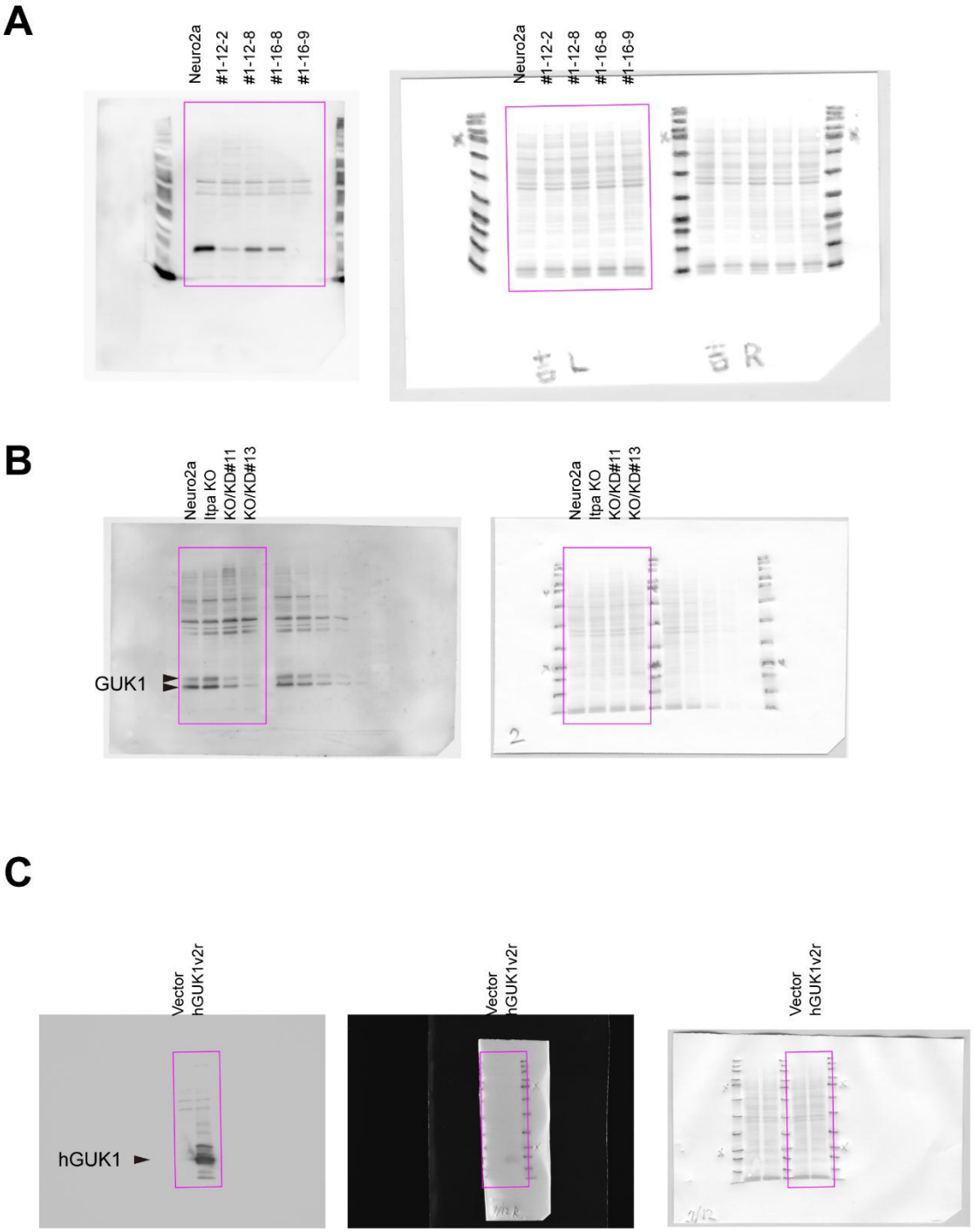

Figure S3. Whole images of western blot signals and Ponceau-S staining images of the membranes.

(A)(B) Whole images of western blot (left) and Ponceau-S staining (right) for Figure 1A (A) and 2A (B) respectively. (C) Whole image of western blot (left), image under LED light (middle), and Ponceau-S staining image (right) for Figure 2E. Red rectangles show the area used in Figure 1A, 2A, and 2E.

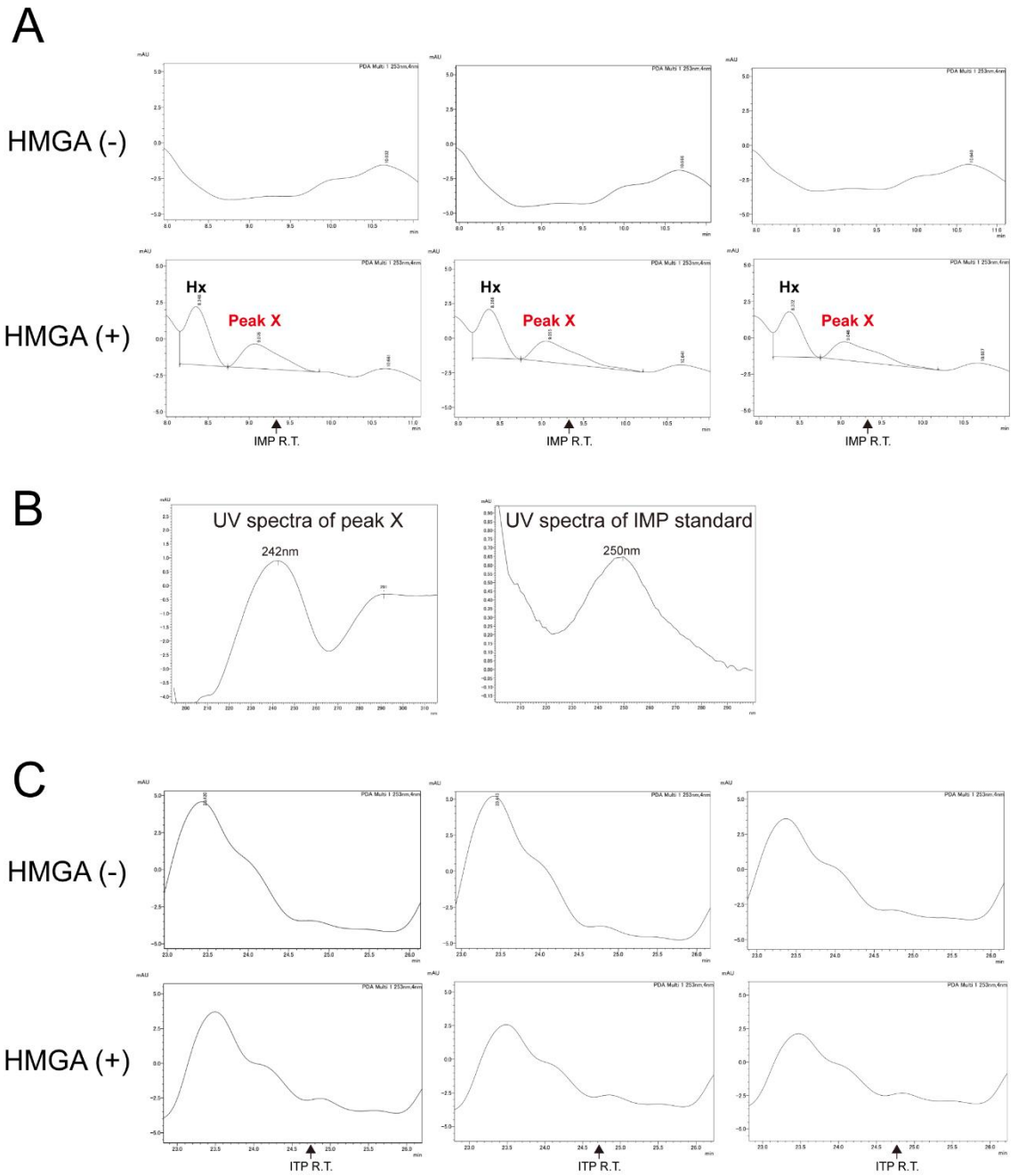

Figure S4. Evaluation of the effects of HMGA-treatment by an HPLC analysis of IMP and ITP in cell extracts.

(A) HPLC chromatographs of extracts from HMGA-treated and untreated cells near retention time (R.T.) of the IMP standard are shown (n = 3). Two HMGA-treatment specific peaks [hypoxanthine (Hx) and unknown peak X] are labeled. (B) UV spectrum of peak X and the IMP standard. (C) HPLC chromatographs of extracts from HMGA-treated and untreated cells near the retention time (R.T.) of the ITP standard are shown (n = 3).

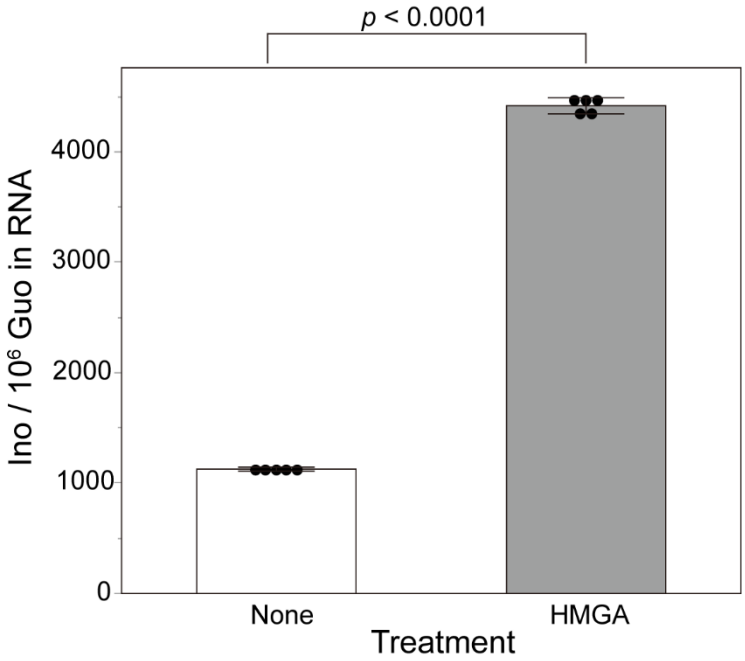

Figure S5. Evaluation of the effect of HMGA-treatment by the inosine level in RNA. Neuro2a *Itpa* KO #1-16-9 clone was cultured for two days with or without HMGA-treatment (n = 5). The inosine levels per 10^6 guanosines in RNA were compared between the two groups. A statistical analysis was performed using Welch's t-test.

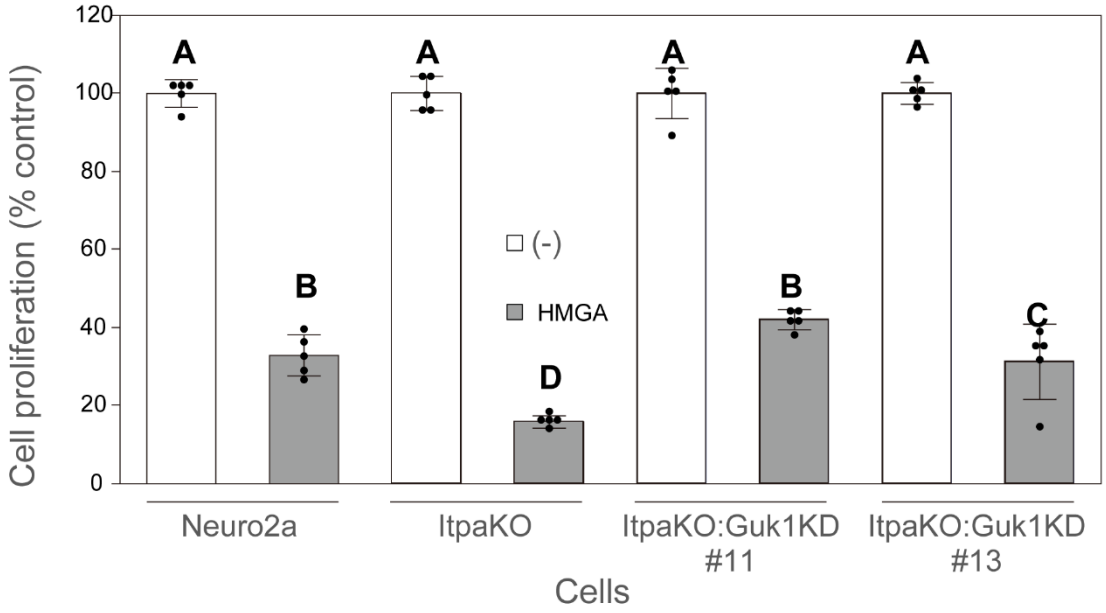

Figure S6. Results of an independent experiment to evaluate the proliferation of *Itpa*-KO/*Guk1*-KD cells cultured with HMGA (hypoxanthine, mycophenolic acid, guanosine, and adenosine).

The graph shows the results of another independent experiment in addition to Figure 2B. A statistical analysis was performed using a 2-way analysis of variance followed by post-hoc Tukey-Kramer honestly significant difference test for multiple comparisons. Bars without the same letters are significantly different.

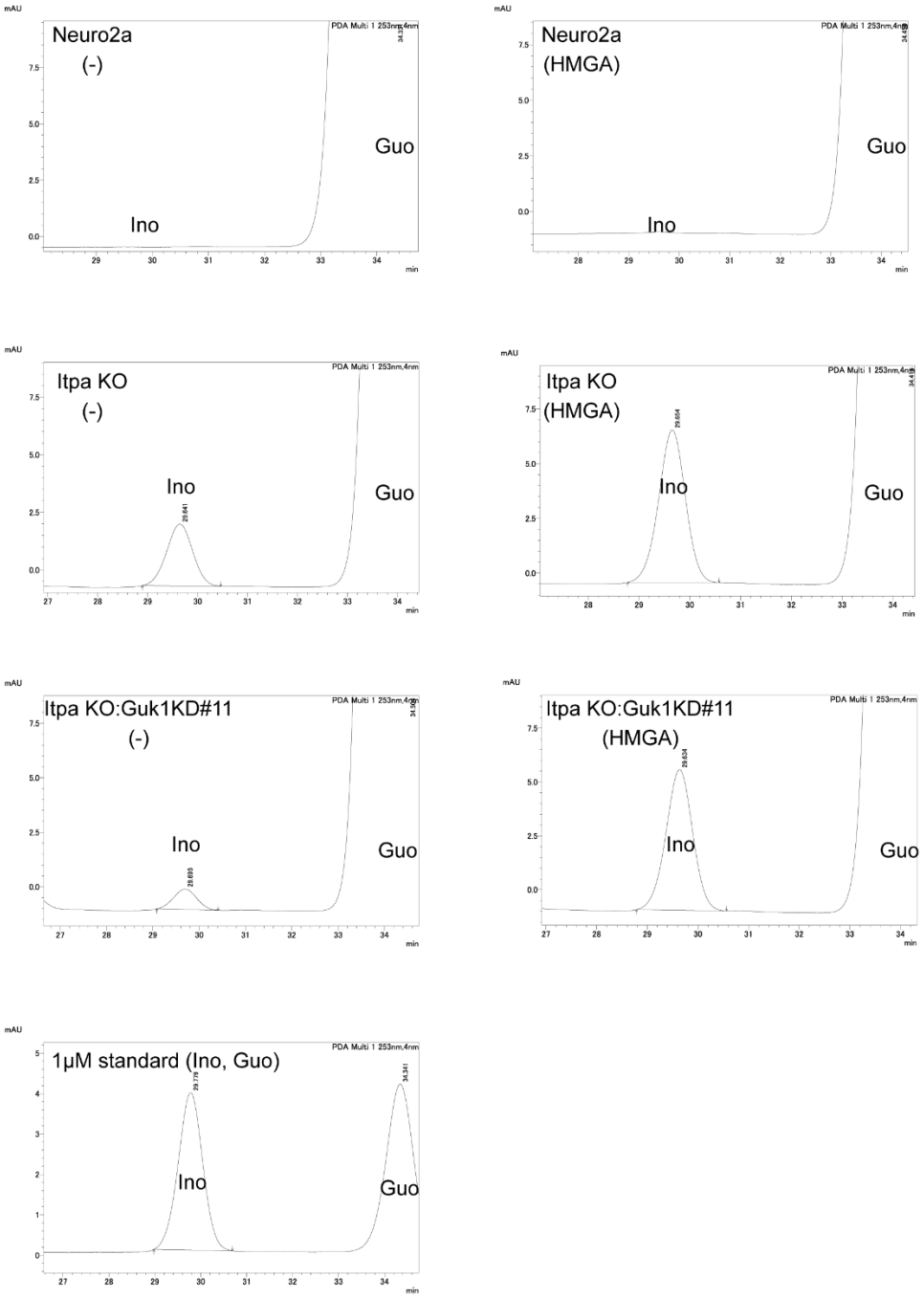

Figure S7. Representative chromatograms of inosine (Ino) and guanosine (Guo) in RNA in a high-performance liquid chromatography analysis. The digested samples were prepared from RNA of Neuro2a, Neuro2a *Itpa*-KO, and Neuro2a *Itpa*-KO/*Guk1*-KD clone #11 treated with or without HMGA (hypoxanthine, mycophenolic acid, guanosine, and adenosine). Positions of inosine (Ino) and guanosine (Guo) peaks in these samples and standard mixture are shown.

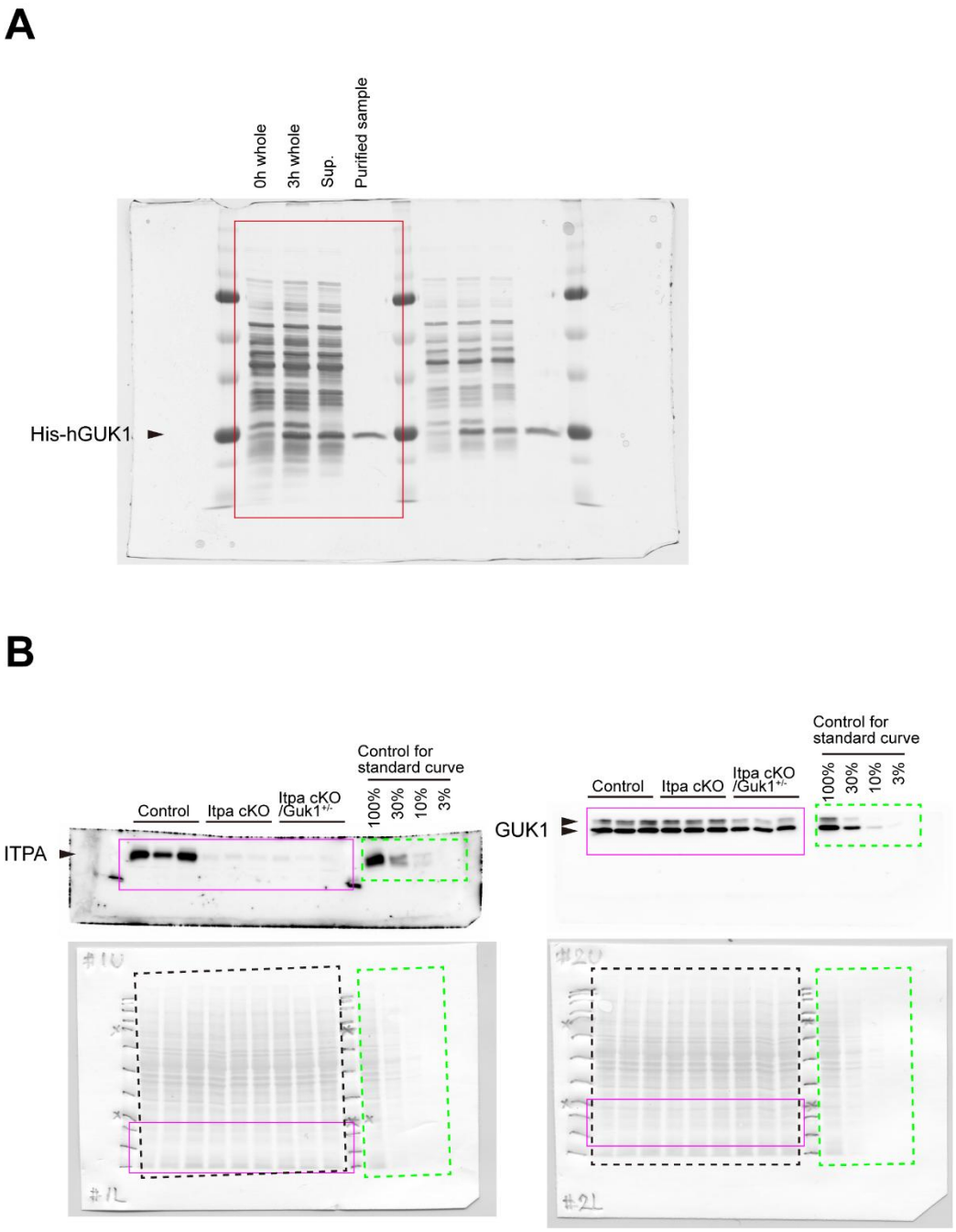

Figure S8. Whole images of silver staining, western blot, and Ponceau-S staining for Figure 3A and 4A.

(A) Whole SDS-PAGE gel image after silver staining. The red rectangle shows the area used in Figure 3A. (B) Whole images of western blots, including lanes for standard curves (upper) and Ponceau S staining (lower). The red rectangles show the areas used for Figure 3A (left) and Figure 4A (right).

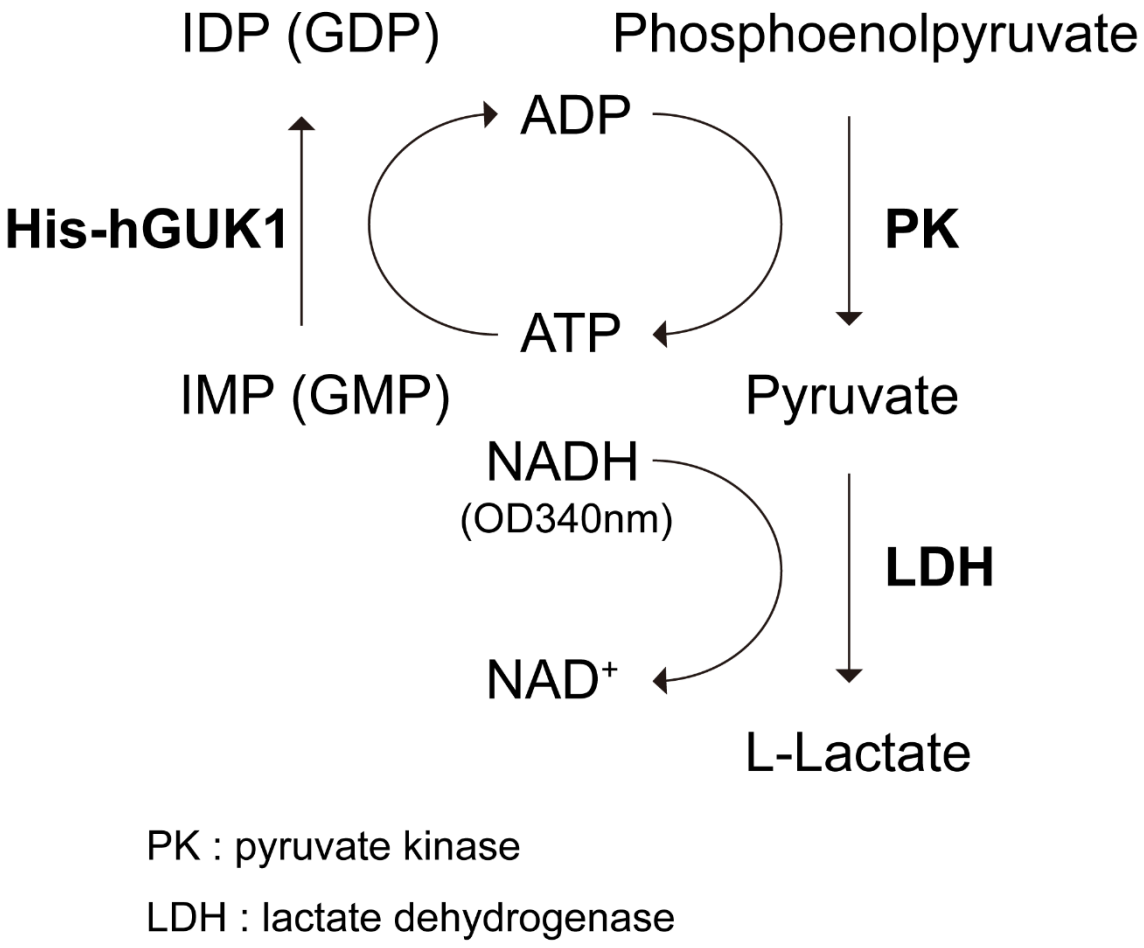

Figure S9. A flow chart of coupled reactions to monitor the phosphorylation reaction of IMP or GMP. ADP, one of the products of GMP/IMP phosphorylation, is used as a substrate of pyruvate kinase (PK). Pyruvate, which is one of product of pyruvate kinase, is used one of substrates of lactate dehydrogenase (LDH). NADH, another substrate of LDH, is also used by the LDH reaction. A decrease of NADH is monitored at OD340.

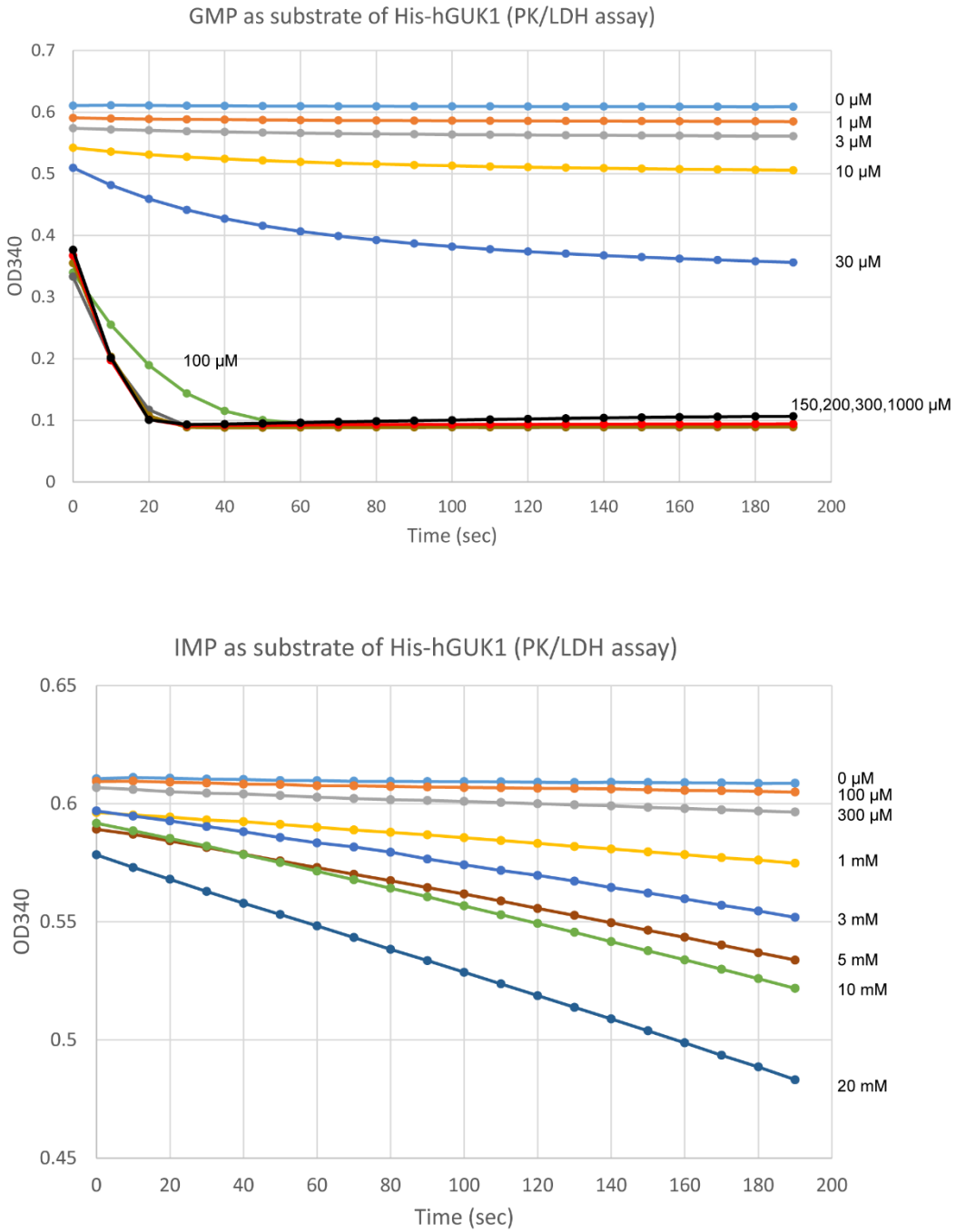

Figure S10. Kinase activity of recombinant His-hGUK1 protein.

The kinase reaction of His-hGUK1 is coupled with pyruvate kinase (PK) and lactate dehydrogenase (LDH) reactions. The coupled reaction was monitored by measuring OD340 of NADH. The mean (n = 3) OD values in monitoring are shown for reactions with various concentrations of guanosine monophosphate (GMP) substrate (upper) and inosine monophosphate (IMP) substrate (lower).

Table S1. Target sequence of the selected 4 shRNAs for mouse *Guk1* gene

Target sequence of the selected shRNAs for mouse *Guk1*	Counts in mModule2-HMGA
GATGGCAAAGATTACTACTTT	45
GAGATGATGCAGCGTGATATT	22
GACGACCTGGATAAAGCCTAT	15
GCAGGCGCTCTCTGAGGAAAT	10

Table S2. Sequences of DNA oligomers

Name	Sequence (5' to 3')
Ex4_1	TGTCTGTGCTTTAACGCACTTGG
Ex4_1 sense	CACCTGTCTGTGCTTTAACGCACTTGG
Ex4_1 anti	AAACCCAAGTGCGTTAAAGCACAGACA
Ex4_target seq Fw3	GTGCACAGAACTGGGAAGGA
Ex4_target seq Rv3	TGCTGATGCCAAGACAGTGA
Ex4_target seq Fw4	ACACAGCCTCTTCTGTTCCA
Ex4_target seq Rv4	TGGGATCCTCCAGGGGTAAA
Fw1 for shRNA with adaptor	[ACACTCTTTCCCTACACGACGCTCTTCCGATCT]-ATTTCTTGGGTAGTTTGCAGTTT
GexSeqN with adaptor	[GTGACTGGAGTTCAGACGTGTGCTCTTCCGATCT]-ACAGTCCGAAACCCCAAACGCACGAA
Target mGuk1variant 5 exon3/4	GATGGCAAAGATTACTACTTT
Guk1 sh ins#1	AAAAGATGGCAAAGATTACTACTTTTTGG-ATCCAAAAAGTAGTAATCTTTGCCATC
Guk1 sh ins#2	AAAAGAGATGATGCAGTGTGATATTTTGG-ATCCAAAATATCACGCTGCATCATCTC
mGuk1 Fw6	CTACAAGGAACCCACGACCT
mGuk1 Rv6	GCTGCAATATCACGCTGCAT
Mmu Rps18-F	AGGATGTGAAGGATGGGAAG
Mmu Rps18-R	ACGAAGGCCCCAAAAGTG
NdeI-hGUK1 Fw	GGACATATGTCGGGCCCCAGGCCTGTGG
hGUK1 Rv-HindIII	AGCAAGCTTCAGGCGCCGGTCCTTTGAGCT
EcoRI-hGUK1 Fw	GGAGAATTCATGTCGGGCCCCAGGCCTGTGG
hGUK1 Rv-NotI	AGCGCGGCCGCTCAGGCGCCGGTCCTTTGAGCT
mGuk1 Fw	TGG GGA CAG TGG TAT CTG TTC
mGuk1 Rv	AGC CGA AAG CCA AAA AGG T

Table S3 Original data of mouse *Guk1* mRNA level and Ino level for figure 2D

Neuro2a Itpa KO/Guk1 KD	Relative mouse *Guk1* mRNA level					Ino / 10^6 Guo in RNA						
Clone #	1st analysis	2nd analysis	mean % control	1st analysis	2nd analysis	3rd analysis	4th analysis	5th analysis	6th analysis	7th analysis	mean	mean % control
#1	0.874	0.870	87.2	836	806						820.67	73.3
#3	1.093	1.018	105.6	1061	1067						1064.08	95.1
#5	0.967	0.940	95.4	852	871						861.48	77.0
#6	1.037	0.991	101.4	943	920						931.21	83.2
#8	0.906	0.896	90.1	766	910						838.29	74.9
#9	0.931	0.967	94.9	901	880						890.58	79.6
#10	1.030	0.963	99.7	940	953						946.56	84.6
#11	0.351	0.285	31.8	440	189	154	130	326	337	300	268.06	24.4
#12	0.912	0.831	87.1	751	749						749.58	67.0
#13	0.085	0.079	8.2	118	124	151	128	107	72	67	109.58	10.0
#14	0.823	0.817	82.0	796	846						820.96	73.4
Control (Neuro2a Itpa KO)	1.000	1.000	100.0	1209	1045	1012	1097	1089	1107	1144	1100.45	100.0

Mouse Guk1 mRNA levels were normalized with internal control Rps18 mRNA level.

Table S4. Ratio of *Guk1* genotypes of newborn mice obtained by mating of $Guk1^{+/-}$male and female mice.

Genotype	Female mice	Male mice	Total	Expected total
$Guk1^{+/+}$	3	9	12	11.5
$Guk1^{+/-}$	18	16	34	23
$Guk1^{-/-}$	0	0	0	11.5

$p = 0.0002$ (Peason's χ^2 test)

Table S5. Number of each genotype of offspring mice obtained by mating with *Itpa*$^{flox/flox}$ and *Itpa*$^{+/flox}$, *Net-Cre*, *Guk1*$^{+/-}$ mice.

Genotype	Female mice	Male mice	Total
Itpa$^{flox/flox}$, *Nes-Cre*, *Guk1*$^{+/+}$	18	12	30
Itpa$^{flox/flox}$, *Nes-Cre*, *Guk1*$^{+/-}$	13	16	29
Itpa$^{flox/flox}$, *Guk1*$^{+/+}$	24	12	36
Itpa$^{flox/flox}$, *Guk1*$^{+/-}$	17	21	38
Itpa$^{+/flox}$, *Nes-Cre*, *Guk1*$^{+/+}$	10	22	32
Itpa$^{+/flox}$, *Nes-Cre*, *Guk1*$^{+/-}$	18	9	27
Itpa$^{+/flox}$, *Guk1*$^{+/+}$	12	18	30
Itpa$^{+/flox}$, *Guk1*$^{+/-}$	16	18	34

$p = 0.8492$ (Peason's χ^2 test)

Reference List for Supplementary Information

1. Naito, Y., Hino, K., Bono, H. and Ui-Tei, K. (2015) CRISPRdirect: software for designing CRISPR/Cas guide RNA with reduced off-target sites. *Bioinformatics* **31**, 1120-1123.
2. Ran, F.A., Hsu, P.D., Wright, J., Agarwala, V., Scott, D.A. and Zhang, F. (2013) Genome engineering using the CRISPR-Cas9 system. *Nat. Protoc.* **8**, 2281-2308.
3. Brinkman, E.K., Chen, T., Amendola, M. and van Steensel, B. (2014) Easy quantitative assessment of genome editing by sequence trace decomposition. *Nucleic Acids Res.* **42**, e168.
4. Behmanesh, M., Sakumi, K., Tsuchimoto, D., Torisu, K., Ohnishi-Honda, Y., Rancourt, D.E. and Nakabeppu, Y. (2005) Characterization of the structure and expression of mouse Itpa gene and its related sequences in the mouse genome. *DNA Res.* **12**, 39-51.
5. Pang, B., McFaline, J.L., Burgis, N.E., Dong, M., Taghizadeh, K., Sullivan, M.R., Elmquist, C.E., Cunningham, R.P. and Dedon, P.C. (2012) Defects in purine nucleotide metabolism lead to substantial incorporation of xanthine and hypoxanthine into DNA and RNA. *Proc. Natl. Acad. Sci. U.S.A.* **109**, 2319-2324.
6. Agarwal, R.P., Scholar, E.M., Agarwal, K.C. and Parks, R.E., Jr. (1971) Identification and isolation on a large scale of guanylate kinase from human erythrocytes. Effects of monophosphate nucleotides of purine analogs. *Biochem. Pharmacol.* **20**, 1341-1354.
7. Ren, H., Wang, L., Bennett, M., Liang, Y., Zheng, X., Lu, F., Li, L., Nan, J., Luo, M., Eriksson, S. *et al.* (2005) The crystal structure of human adenylate kinase 6: An adenylate kinase localized to the cell nucleus. *Proc. Natl. Acad. Sci. U.S.A.* **102**, 303-308.
8. Lascu, I. and Gonin, P. (2000) The catalytic mechanism of nucleoside diphosphate kinases. *J. Bioenerg. Biomembr.* **32**, 237-246.
9. Lu, Q. and Inouye, M. (1996) Adenylate kinase complements nucleoside diphosphate kinase deficiency in nucleotide metabolism. *Proc. Natl. Acad. Sci. U.S.A.* **93**, 5720-5725.
10. Schaertl, S., Konrad, M. and Geeves, M.A. (1998) Substrate specificity of human nucleoside-diphosphate kinase revealed by transient kinetic analysis. *J. Biol. Chem.* **273**, 5662-5669.